First published online as a Review
in Advance on May 21, 2007

Cold Dark Clouds: The Initial Conditions for Star Formation

Edwin A. Bergin[1] and Mario Tafalla[2]

[1]Department of Astronomy, University of Michigan, Michigan, 48109;
email: ebergin@umich.edu

[2]Observatorio Astronómico Nacional, E-28014 Madrid, Spain;
email: m.tafalla@oan.es

Key Words

interstellar medium, interstellar molecules, molecular clouds, prestellar cores, star formation

Abstract

Cold dark clouds are nearby members of the densest and coldest phase in the Galactic interstellar medium, and represent the most accessible sites where stars like our Sun are currently being born. In this review we discuss recent progress in their study, including the newly discovered IR dark clouds that are likely precursors to stellar clusters. At large scales, dark clouds present filamentary mass distributions with motions dominated by supersonic turbulence. At small, subparsec scales, a population of subsonic starless cores provides a unique glimpse of the conditions prior to stellar birth. Recent studies of starless cores reveal a combination of simple physical properties together with a complex chemical structure dominated by the freeze-out of molecules onto cold dust grains. Elucidating this combined structure is both an observational and theoretical challenge whose solution will bring us closer to understanding how molecular gas condenses to form stars.

1. INTRODUCTION: HOLES IN THE HEAVENS

"Hier ist wahrhaftig ein Loch im Himmel!" or "Here is truly a hole in the heavens!," William Herschel was heard by his sister Caroline to exclaim in 1784 when he pointed his telescope toward the constellation Scorpius and viewed the dark nebulae in Ophiuchus (Houghton 1942). Herschel reported his discovery the following year (Herschel 1785), and for the next century astronomers debated whether these dark objects were truly voids, left by the stars as theorized by Herschel, or were perhaps nebulous dark regions observed projected upon a dense and bright stellar background. Our views began to change when Edward Emerson Barnard, who was motivated by Herschel's discovery, published the first modern and systematic photographic survey of the "Dark Markings of the Sky" (Barnard 1919). Barnard argued that his deep photographs provided increasing evidence that many of these dark areas were "obscuring bodies nearer to us than the distant stars."

Such regions might have remained just obscured curiosities were it not for the clear association with star formation, which began to be recognized in the middle of the twentieth century. The first person to recognize this was Bart J. Bok in 1946 (Bok 1948) when he claimed that the dark nebula, in particular compact and nearly round ones that now bear the name "Bok Globules," are the sites of stellar birth. It was the advent of modern infrared (IR) and millimeter-wave technology in the latter half of the twentieth century that cemented the relationship between dark clouds and the formation of stars and planetary systems.

The discovery of molecules in space further revealed that dark clouds are made of molecular material with H_2 as the dominant constituent (Weinreb et al. 1963, Wilson et al. 1970). Since this finding, the terms molecular cloud and dark cloud are often used interchangeably, as they refer to the two main characteristics of the clouds: their molecular composition and their opaque optical appearance. Molecular clouds are dark not because of their hydrogen molecules, but because of a population of tiny solids (dust grains) that absorb the optical starlight and lead to high visual extinctions ($A_V > 1^m$). Such a dimming of the starlight reduces the heating effects from external radiation and results in temperatures a few degrees above the 2.7 K cosmic background.

For the purpose of this review we will use the term cold dark cloud to refer to those molecular clouds that are close enough (<500 pc) to be seen in silhouette against the background Galactic starlight. These clouds (e.g., Taurus, Perseus, Ophiuchus, Lupus, ...) are observed to be forming low-mass stars either in isolation or in small compact groups and have gas temperatures ∼10 K to 20 K. This stands in contrast to diffuse clouds in the Milky Way, which contain molecular material but are not forming stars and are not optically opaque with $A_V < 1^m$. At the other end of the spectrum of Galactic star formation lies the more distant and more massive giant molecular clouds that form rich stellar clusters and contain embedded massive stars that heat the surrounding gas to temperatures >20 K.

Over the past decade the development of sensitive continuum and heterodyne detectors at millimeter and submillimeter wavelengths has led to clear and important advances in our knowledge of the physics and chemistry of these cold dark clouds.

Particular progress has been made in the study of regions prior to onset of star formation, which is the primary focus of this review. We will first discuss the gains in our knowledge starting from the larger tens to hundreds of parsec scale of molecular clouds. We will follow with a detailed discussion of the physics and chemistry of the much smaller, ~ 0.1 pc, scale of molecular cloud cores, where recent research has clarified a number of outstanding issues. We conclude with a discussion of a newly discovered class of cold ($T_{gas} \sim 10$ K to 20 K) dark clouds: IR dark clouds that represent a new population of dense molecular regions and are believed to be the precursors to stellar clusters and massive stars.

Space constraints prohibit this review from complete coverage of the formation of clouds, stars, and planets. For more details we refer the reader to recent reviews of star formation [Larson 2003; see also the review by McKee & Ostriker (2007) in this volume], the role of turbulence (Elmegreen & Scalo 2004, Mac Low & Klessen 2004), probes of physical conditions (Evans 1999), gas/dust chemistry and star formation (van Dishoeck & Blake 1998, Ehrenfreund & Charnley 2000, van Dishoeck 2004), and the entire *Protostars and Planets V* volume (Reipurth et al. 2007), especially the papers by Ceccarelli et al. (2007), Di Francesco et al. (2007), and Ward-Thompson et al. (2007) therein that contain complementary reviews of this topic and include references that, for reasons of limited space, could not be mentioned here. Recent accounts of how the new observations with the *Spitzer Space Telescope* (*Spitzer*) are advancing our knowledge of star formation in dark clouds can be found in Werner et al. (2006) and Allen et al. (2007).

Although recent progress clearly warrants this review, the year 2007 presents an auspicious occasion for an overview of dark clouds. It is 150 years since the birth of E.E. Barnard in Nashville in December 1857, 101 years since the birth of B.J. Bok in the Netherlands, and 80 years since Barnard's *Photographic Atlas of Selected Regions of the Milky Way* was published posthumously (Barnard 1927). It is also the centennial of Barnard's beautiful exposure of Taurus-Auriga, which is shown in **Figure 1**. The hundred years that separate us from Barnard's picture of Taurus have brought us a wealth of knowledge on the physics and chemistry of these dark patches. As we will see in this review, however, dark clouds remain in some aspects as mysterious and fascinating as when Barnard pointed his camera to them.

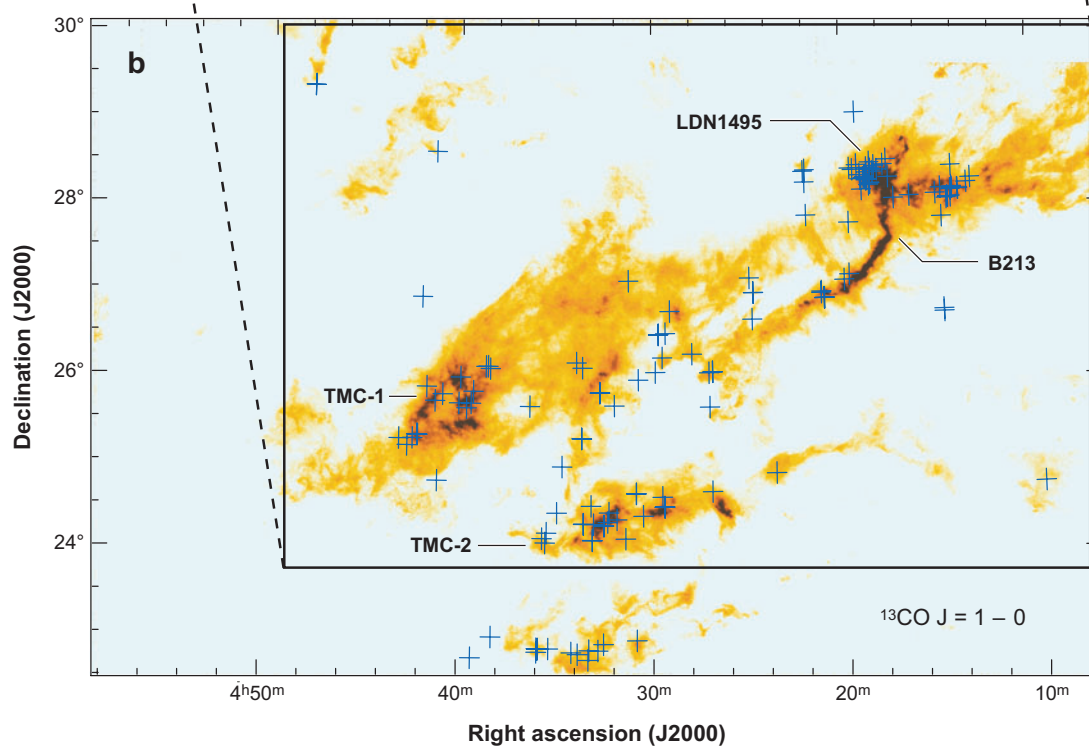## 2. LARGE SCALE STRUCTURE OF COLD DARK CLOUDS

2.1. Recent Studies

A number of technical developments over the past decade have rapidly increased our ability to study dark clouds. Large-scale digital images in the optical, IR, and radio regimes have become available on a routine or quasi-routine basis, and their analysis allows studying degree-sized portions of the sky at arcminute or better resolution. In the following sections we review some of these developments ordered by wavelength, and we briefly discuss the analysis techniques used to exploit this new wealth of data. Thanks to this recent progress, the study of cloud structure is currently enjoying a new golden age.

a

E.E. Barnard: Nebulous Region in Taurus (January 1907)

b

LDN1495

B213

TMC-1

TMC-2

$^{13}CO\ J = 1 - 0$

Declination (J2000)

30°

28°

26°

24°

4ʰ50ᵐ   40ᵐ   30ᵐ   20ᵐ   10ᵐ

Right ascension (J2000)

2.1.1. Optical and infrared data. The Digitized Sky Survey (DSS) and the USNO Precision Measuring Machine project (USNO-PMM; Monet 1996) have provided multi-band, all-sky images at optical wavelengths with accurate calibration and registration. Using different techniques, these data can be processed automatically to create large-scale images of dark clouds. Cambrésy (1999) has used USNO-PMM data together with a star-counting method to produce extinction (A_V) maps of up to ~250 square degrees for 24 dark clouds including Taurus, Perseus, and Ophiuchus. He has used an automatic adaptive grid with a fixed number of stars per cell to avoid empty pixels and to achieve a maximum extinction of around $A_V \sim 7$ mag. This adaptive cell method, however, degrades the angular resolution of the images from about 1 arcmin in the outer parts of the clouds to about 10 arcmin in the most opaque areas. A similar star-counting technique, but with a fixed cell spacing, has been used by Dobashi et al. (2005) to make an atlas of dark clouds using DSS-I data. These researchers identify 2448 dark clouds toward the Galactic plane ($b \leq 40°$) and present maps with angular resolutions of 6 arcmin and 18 arcmin that are publicly available (**http://darkclouds.u-gakugei.ac.jp**).

Near-IR observations can be used to extend the optical extinction measurements to the most opaque regions of clouds thanks to the wavelength dependence of the dust absorption. The recent development of large-format IR arrays has made it possible to apply this technique to increasingly large regions of the sky, and thus complement the work carried out at optical wavelengths. In addition to applying the star-count method, which provides an estimate of the average extinction inside a grid cell, multiband near-IR observations can be used to provide a direct determination of the extinction toward individual background stars. This determination uses the small range of near-IR colors spanned by the background stars (mostly giants), which for practical purposes and with little error can be assumed constant. The Near Infrared Color Excess (NICE) method of Lada et al. (1994) uses H and K observations of background stars together with an estimate of their intrinsic (H-K) color from a nearby unobscured control field to derive A_V for each observed star. As an application of this method, Lada et al. (1994) produced an accurate map of the extinction toward the IC 5146 dark cloud with a resolution of 1.5 arcmin (also Lada, Alves & Lada 1999). An improvement of this technique is the NICER (NICE Revisited) method of Lombardi & Alves (2001), which uses observations in additional near-IR bands to reduce the variance of the A_V estimate. By applying this method to the Orion data of the all-sky 2MASS survey (Skrutskie et al. 2006), these authors show that it is possible

←——

Figure 1

(*a*) Photographic image of the Taurus Molecular Cloud taken by E.E. Barnard (Barnard 1919). His notes state that, "very few regions of the sky are so remarkable as this one. Indeed the photograph is one of the most important of the collection, and bears the strongest proof of the existence of obscuring matter in space." Courtesy of the Observatories of the Carnegie Institution of Washington. (*b*) ^{13}CO J = 1–0 integrated emission map of the same region obtained using the Five College Radio Astronomy Observatory. Blue crosses mark the location of known stellar and protostellar objects and the emission color scale ranges from 0.5 to 10 K km s^{-1}. Image kindly provided by P.F. Goldsmith in advance of publication.

to derive large-scale cloud structure with 5 arcmin resolution to a limiting extinction of $A_V \approx 0.5$ mag (better or comparable to optical star-count work and below the threshold for molecular CO formation). Future use of this technique with 8-m class telescopes is expected to provide accurate extinction maps with two orders of magnitude dynamical range and a resolution better than 10 arcsec (Lombardi & Alves 2001).

2.1.2. Radio data. In parallel with the technical advances in near-IR cameras, millimeter- and submillimeter-wavelength bolometer arrays have grown in size and sensitivity over the past decade. Arrays like Submillimetre Common-User Bolometer Array (SCUBA) on the James Clerk Maxwell Telescope (JCMT), the Max Planck Millimetre Bolometer Array (MAMBO) on the Institut de Radio Astronomie Millimétrique (IRAM) 30-m telescope, and Bolocam on the Caltech Submillimeter Observatory (CSO) have made it possible to map systematically the thermal emission of cold dust from dark clouds (e.g., Motte, André & Neri 1998; Johnstone et al. 2000; Enoch et al. 2006). In contrast with their near-IR counterpart, however, millimeter and submillimeter observations of dark clouds are sensitive to a narrower range of dust temperatures and suffer from severe instrumental limitations. The need to chop the telescope between sky and reference positions filters out part of the large-scale emission, which is usually weak enough to be close to the detection limit of the array. This means that bolometer observations miss most of the extended emission from a cloud while they recover its full small-scale structure. The future SCUBA-2 array at the JCMT, with its expected thousand-fold increase in mapping speed and high sensitivity for extended emission, promises to revolutionize the field of dust continuum mapping of dark clouds.

Molecular-line observations, on the other hand, provide information about the gas component of clouds, in particular about their velocity structure, density, temperature, and chemical composition. These data are complementary to the dust extinction and emission measurements, and they are required to understand, among other issues, the equilibrium status and the chemical evolution of dark clouds. Progress in millimeter-line receiver technology over the past ten years has also improved our ability to map large areas of the sky with increasing angular and spectral detail. Low-resolution ($\approx$10 arcmin) CO imaging of the entire Milky Way has been carried out with the CfA 1.2-m telescope (Dame, Hartmann & Thaddeus 2001), and systematic mapping of selected clouds at higher resolution ($\approx$2 arcmin) has been performed in CO isotopologues with the NANTEN/Nagoya 4-m telescope (e.g., Tachihara et al. 2002) and the KOSMA 3-m telescope (e.g., Sun et al. 2006). The 32-beam SEQUOIA array (and its predecessor, the 15-beam QUARRY array), operating at 3 mm on the FCRAO 14-m telescope, have been used to make megapixel images with subarcminute resolution of nearby clouds like Taurus (**Figure 1** and Goldsmith et al. 2005) and further-out regions like the Galactic Ring (Jackson et al. 2006) and the outer Galaxy (Heyer et al. 1998). This array has also provided line data for the Coordinated Molecular Probe Line Extinction and Thermal Emission (COMPLETE) project (Ridge et al. 2006), which has the goal of combining the different IR and radio techniques of dark cloud mapping to study a series of dark clouds common to the *Spitzer* Legacy Program "From Molecular Cores to Planet Forming Disks"

(c2d, Evans et al. 2003). The potential of heterodyne arrays, however, has not been fully exploited yet because the reduced number of pixels in the receivers limits the large-scale observations to the bright lines of CO isotopologues. Further progress in this technology is still crucial to our understanding of the large-scale physics and chemistry of dark clouds.

2.2. Observational Properties of Dark Clouds

The dark cloud data obtained using the new instrumentation complements a large body of previous work summarized in previous reviews like those by Goldsmith (1987), Lada, Strom & Myers (1993), and Myers (1995). These new data have helped greatly to refine our understanding of the dark cloud properties, although, as we will see, a number of important uncertainties still remain. In the following sections, we review some of the basic properties of clouds with emphasis on recently clarified issues and general characteristics from an observational point of view, concluding with a brief review of the issues whose solutions remain pending. Because of space limitations, we cannot do justice to all the excellent studies of individual clouds carried out with the optical, IR, and radio instrumentation discussed above.

2.3. Shapes

A simple inspection of dark cloud images obtained by any of the methods discussed above reveals that clouds come in a variety of sizes and shapes. In general, dark clouds have highly irregular edges, and their overall appearance is filamentary and often wind-blown. The presence of long, well-defined filaments was emphasized already a century ago by Barnard (1907) when he noted, describing the Taurus plate of **Figure 1**, that "among the most surprising things in connection with these nebula-filled holes are the vacant lanes that so frequently run from them for great distances." Indeed, some of the filaments in Taurus can be followed for more than 4° or 10 pc, and similarly thin and long structures can be seen in many other clouds like Ophiuchus, Lupus, and Orion both in optical plates (Schneider & Elmegreen 1979) and radio images (Bally et al. 1987, Johnstone & Bally 1999).

In many clouds including Taurus and Ophiuchus, the length of some filaments is comparable to the full extent of the cloud. Typically, a cloud contains two or three long filaments that are either parallel or converge at a low angle in a massive condensation that often contains an active cluster-forming site (Tachihara et al. 2002, Burkert & Hartmann 2004). The velocity field of some filaments, in addition, seems rather coherent (see Loren 1989, for a study of Ophiuchus). This combination of spatial length and velocity coherence for some of the filaments suggests that their presence is intrinsic to the cloud structure and not the result of later evolutionary factors like star-formation activity, which would produce a more chaotic, small-scale mass distribution. Dark clouds, therefore, seem to be born with a filamentary distribution of material that extends over a number of parsecs. As clouds evolve and form stars, the products of star formation inherit the filamentary distribution of the parental gas (Hartmann 2002).

2.4. Mass Distribution

Maps of dark clouds provide more than just information on shapes. Measurements of dust extinction or gas column density at each cloud position can be used to estimate the amount of material under different physical conditions, and in particular at different densities. In his extinction study of 24 dark clouds, Cambrésy (1999) finds that most of them present a similar power-law relation between the mass enclosed in an iso-extinction contour and the extinction, although the A_V range of this optical study is restricted to $A_V \approx 1$ to 5 mag. Despite this limitation, the measurements illustrate how most of the material in a cloud lies at relatively low extinctions, and it must therefore reside in the form of low-density gas. Using more sensitive near-IR extinction data, Alves, Lada & Lada (1999) find that only 25–30% of the total mass in the IC 5146 and L977 cloud lies at $A_V > 10$ mag, whereas Cambrésy et al. (2002) finds that this percentage is slightly more than 10% for the North America Nebula. A much smaller value (∼1%) has been recently reported for the Pipe Nebula, also from IR extinction measurements (Lombardi, Alves & Lada 2006, also Lada, Alves & Lombardi 2007). Similar low fractions of dense material are indicated by large-scale maps of dust emission in clouds actively forming stars. Johnstone, Di Francesco & Kirk (2004) and Young et al. (2006) find that only between 1% and 2% of the mass in the Ophiuchus cloud is associated with dense, submillimeter continuum emission, and that this emission is only detected toward regions of extinction larger than 10–15 mag. This is illustrated in **Figure 2**, which shows the IR-extinction and submillimeter-emission maps of Ophiuchus from Young et al. (2006).

A related measure of how the mass of a cloud is distributed among different regimes is the statistics of extinction values. Ridge et al. (2006) find lognormal distributions for the number of pixels as a function of extinction in both Perseus and Ophiuchus, a distribution that is in agreement with the prediction of turbulent models of cloud formation (Vazquez-Semadeni 1994, Ostriker, Stone & Gammie 2001). Lombardi, Alves & Lada (2006), in their study of the Pipe Nebula, find that although a lognormal distribution provides an approximate general fit to the data, the observed histogram has significantly more structure that can only be reproduced with additional components.

2.5. Velocity Structure

The presence of supersonic motions in dark clouds has been known since the first molecular-line studies revealed non-Gaussian line shapes and velocity differences across clouds of the order of 1 km s^{-1} or more (sound speed is 0.2 km s^{-1} for 10 K gas). These motions are inferred to be turbulent from the lack of systematic patterns like rotation, expansion, or infall (Heiles & Katz 1976), and from the existence of a systematic power-law relation between the velocity dispersion inside a cloud σ and its physical size $L[\sigma(\text{km s}^{-1}) = 1.10L(\text{pc})^{0.38}$, Larson 1981], which is reminiscent of the classical Kolmogorov law of (incompressible) turbulence. Understanding and characterizing these turbulent motions, which affect not just dark clouds but the whole interstellar medium at almost every scale, is a formidable task. In contrast with their laboratory counterparts, turbulent motions in the interstellar medium are
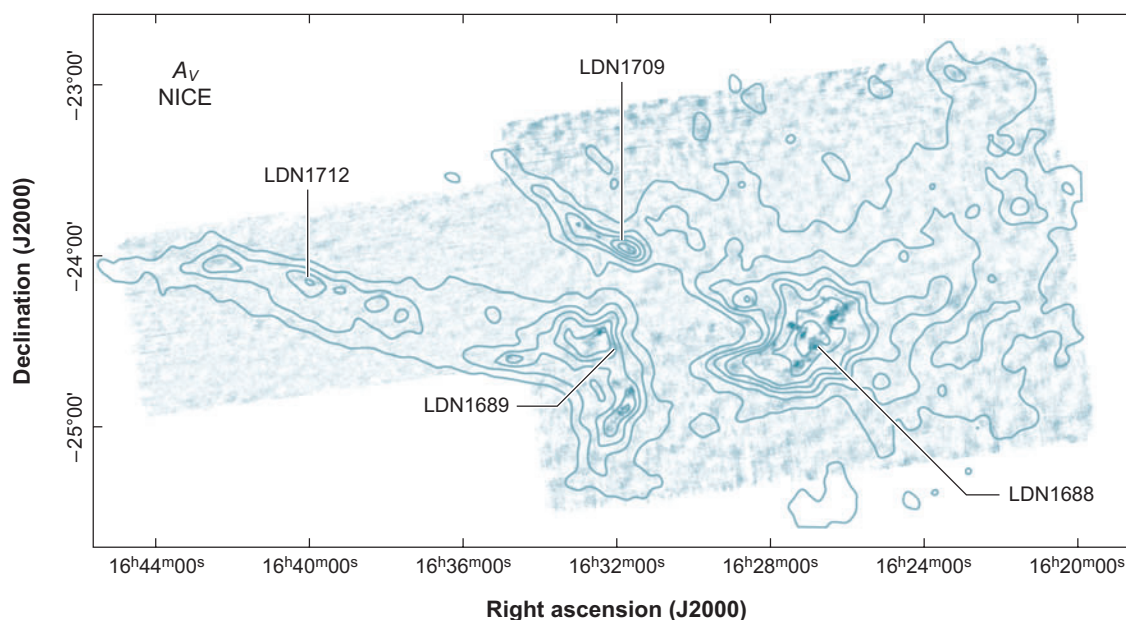
Figure 2

Maps of IR extinction (contours) and submillimeter emission (*blue shading*) for the ρ Ophiuchus dark cloud illustrating how the dense gas, responsible for the submillimeter continuum emission, represents a small fraction of the total amount (and an even smaller fraction of the total volume). Most of the gas in the cloud is in the form of low-density, low-extinction gas. Contours are at $A_V = 2$, 4, 6, 8, 10, 15, and 20 mag with an effective resolution of 5 arcmin. Figure from Young et al. (2006).

supersonic, compressible, and likely of magnetohydrodynamical nature. A rich field of both analytic and numerical work has been developed to tackle this problem, and a review of the results exceeds the scope of this review. We refer the reader to the excellent recent review by Elmegreen & Scalo (2004) for an in-depth view of interstellar turbulence, especially from a theoretical point of view, and for an extensive list of references. Here we will concentrate on the main observational results of recent studies of dark cloud kinematics.

When studying the kinematics of cloud gas, it is necessary to take into account its dependence on density. Models of compressible supersonic turbulence show that the highest density gas moves slower than the low-density material, as it arises from the convergence of flows (Padoan et al. 2001), and this velocity segregation seems to be present in clouds. The densest regime in a cloud corresponds to the dense cores, which are known to have very low levels of turbulence and subsonic internal motions (Myers 1983). Dense cores seem therefore to lie at the bottom of the hierarchy of cloud kinematics, and to represent structures dominated by the dissipation of turbulence (Goodman et al. 1998). In Section 3 we will present a more complete summary of the physical properties of dense cores and defer the discussion of dense gas kinematics to that section.

The kinematics of the low-density gas in dark clouds at the small scales typical of dense cores ($\sim$0.1 pc) has been studied in detail by Falgarone et al. (1998). These researchers selected three regions in nearby clouds and mapped them in different CO isotopologues over several arcminutes (tenths of a parsec for the clouds' distance) with the IRAM 30-m telescope. Each selected region contains a starless dense core, although the CO emission is dominated by the more diffuse material because of optical depth and depletion effects (see Section 4.2). Even at their limit of angular resolution (about 1700 AU), Falgarone et al. (1998) find unresolved velocity structure, especially at the highest speeds. This fastest gas appears as prominent wings in non-Gaussian CO spectra with velocities of about 1 km s^{-1} and has an extremely filamentary distribution with aspect ratios larger than about 5. In contrast with the dense (10^5 cm^{-3}), subsonic gas in a core, the fast CO-emitting gas (with a density of a few 10^3 cm^{-3}) presents large shears and velocity dispersions at the smallest resolvable spatial scales. The small regions of high shear may represent locations of enhanced dissipation of turbulence (Pety & Falgarone 2003).

The large-scale distribution of turbulence in clouds has been studied by a number of researchers using different techniques. In addition to the classical linewidth-size relation of Larson (1981), methods used to analyze cloud kinematics include the statistics of the centroid velocity fluctuations (Miesch, Scalo & Bally 1999), the spectral correlation function (SCF, Rosolowsky et al. 1999), the principal component analysis (PCA, Heyer & Schloerb 1997), and the velocity channel analysis (VCA, Lazarian & Pogosyan 2000). A common goal of these methods is to identify and extract from maps of molecular-line emission a number of statistical properties of the velocity field that can be compared with the expectations from analytic theory (like Kolmogorov's law) or from numerical simulations of hydrodynamic and magnetohydrodynamic turbulence (Ossenkopf & Mac Low 2002, Ballesteros-Paredes et al. 2007). Two main issues addressed by these studies are the way in which the turbulent energy is distributed between the different spatial scales [as described by the energy spectrum $E(k)$] and the nature of the driving agent (for more details, see Elmegreen & Scalo 2004).

A recent example of the above type of work is the principal component analysis of 23 fields of the FCRAO CO Outer Galaxy Survey by Brunt & Heyer (2002). Using these and additional data, Heyer & Brunt (2004) have found an almost universal power-law form for the energy spectrum of clouds, with very little cloud-to-cloud scatter (10–20%) not only in the power-law index but in the normalization coefficient. Such little scatter would help explain the emergence of Larson's law when combining data from an ensemble of clouds (Larson 1981). By combining numerical simulations of supersonic turbulence with an analysis of the velocity line centroid, the linewidth-size relation, and the PCA determinations of turbulence properties, Brunt & Mac Low (2004) suggest that observations of line emission from clouds are best fitted by compressible, shock-dominated (Burgers) turbulence. They also suggest that clouds are either recently formed or they are continually driven on large scales. These suggestive results still need confirmation from the systematic observation of a large number of nearby clouds and from the realistic modeling of the combined effect of cloud kinematics, chemistry, and radiative transfer. The extreme complexity of turbulent motions in clouds, the diverse mechanisms likely involved in their driving and dissipation,

and the challenge of obtaining high-quality molecular-line data of whole clouds will surely continue to challenge theorists and observers alike for a number of years.

2.6. Internal Structure

A common feature of dark clouds is that they show a partly hierarchical structure, with smaller subunits appearing within large ones when observed with increasing spatial resolution. To characterize this structure, two different approaches have been generally followed, depending on whether the discrete or the continuous nature of the structure is emphasized. In the first approach, the cloud is assumed to be composed of subunits, referred to as clumps and defined as coherent regions in position-velocity space that may contain significant substructure (Williams, Blitz & McKee 2000) (see below and **Table 1** for typical clump parameters). These clumps are identified from the data using an automatic clump-finding algorithm that simplifies the process and avoids human bias. The most popular algorithms in use are GAUSSCLUMPS, developed by Stutzki & Güsten (1990), and CLUMPFIND from Williams, de Geus & Blitz (1994). These algorithms follow different approaches to identify and characterize clumps, but they generally agree in the derived properties, especially in the intermediate- and high-mass end (Williams, de Geus & Blitz 1994). When they are applied, usually to CO isotopologue data, the spectrum of clump properties is found to follow a power law in the range for which the data are complete. The mass of the clumps, for example, commonly presents a distribution of the form $dN/dM \sim M^{-\alpha}$, where α lies in a narrow range between 1.4 and 1.8 for both dark clouds and giant molecular clouds (Blitz 1993, Kramer et al. 1998). As a reference, and in this form, we note that the initial mass function of stars follows a steeper power law with a slope of $\alpha = 2.35$ (Salpeter 1955). The clump distribution, therefore, contains most of the mass in massive clumps, whereas the stellar distribution has most of the mass in low-mass objects.

Table 1   Properties of dark clouds, clumps, and cores

	Clouds[a]	Clumps[b]	Cores[c]
Mass ($M_\odot$)	$10^3 - 10^4$	50–500	0.5–5
Size (pc)	2–15	0.3–3	0.03–0.2
Mean density (cm^{-3})	50–500	10^3–10^4	10^4–10^5
Velocity extent (km s^{-1})	2–5	0.3–3	0.1–0.3
Crossing time (Myr)	2–4	≈1	0.5–1
Gas temperature (K)	≈10	10–20	8–12
Examples	Taurus, Oph,	B213, L1709	L1544, L1498,
	Musca		B68

[a]Cloud masses and sizes from the extinction maps by Cambrésy (1999), velocities and temperatures from individual cloud CO studies.
[b]Clump properties from Loren (1989) (^{13}CO data) and Williams, de Geus & Blitz (1994) (CO data).
[c]Core properties from Jijina, Myers & Adams (1999), Caselli et al. (2002a), Motte, André & Neri (1998), and individual studies using NH_3 and N_2H^+.

The second approach to characterize cloud structure assumes that the cloud is self-similar, at least over some range of scales, and applies the concepts of fractal geometry. In this geometry, the most characteristic parameter of an object is its fractal (or Hausdorff) dimension, which is not, in general, an integer number (Mandelbrot 1983). The boundary of a cloud, for example, has a fractal dimension D_p that can be estimated from the relation between the enclosed area (A) and the perimeter length (P): $P \sim A^{D_p/2}$ (Lovejoy 1982). For simple curves in a plane, like circles or ellipses, this area-perimeter relation gives the expected value of $D_p = 1$ for the dimension of a line. For highly fragmented or convoluted curves, the expression gives a value that is larger than 1 and that approaches 2 as the curve fills a larger fraction of the plane. Beech (1987) used the above area-perimeter relation for the optical boundary of 24 dark clouds and derived an average boundary dimension of 1.4, which suggests that clouds are fractal. Using a similar method for the iso-contours of a series of CO maps, Falgarone, Phillips & Walker (1991) have derived a bounday dimension $D_p = 1.36 \pm 0.02$ for the Taurus molecular cloud, almost the same value measured by Scalo (1990) from *Infrared Astronomical Satellite* (IRAS) maps. Similar values for the fractal dimension have been obtained for the more diffuse cirrus clouds ($D_p = 1.3$, Bazell & Desert 1988) and even for the atmospheric clouds on Earth ($D_p = 1.35$, Lovejoy 1982). As these dimension estimates use plane-of-the-sky views or maps of the objects, they only provide the fractal dimension of the clouds projection. To infer the intrinsic (volume) fractal dimension, the area-perimeter value is generally increased by 1 (Beech 1992), although this procedure may only provide a lower limit to the true dimension (Sánchez, Alfaro & Pérez 2005). With this assumption, the area-perimeter determinations imply a typical cloud fractal dimension of around $D = 2.4$.

The very different approaches of the clump-finding and fractal analysis would seem to suggest that the two methods provide contradictory views of the cloud internal structure. This is however not the case, as the power-law behavior found in the spectra of clump properties already suggests a scale-free structure consistent with a fractal geometry (Elmegreen & Falgarone 1996, also Stutzki et al. 1998). Indeed, Elmegreen & Falgarone (1996) show that it is possible to derive clump mass distribution functions as those found by the GAUSSCLUMPS and CLUMPFIND algorithms from fractal cloud models of (volume) dimension $D = 2.3 \pm 0.3$. In this view, the clump-finding algorithms identify the peaks of the fractal intensity distribution of a cloud. Owing to the threshold imposed in the density or column density by the observations, a power-law spectrum of cloud sizes results, and this produces a power-law distribution of clump masses even if the gas density follows a lognormal distribution (Elmegreen 2002).

The self-similar behavior revealed by both the power-law clump decomposition and the fractal description seems to apply inside a given range of spatial scales. This range most likely represents the regime dominated by turbulent motions, as turbulence produces self-similar structures in a natural way (e.g., Elmegreen & Scalo 2004). At large scales, the presence of well-defined features like filaments or shells indicates a deviation from self-similarity that is likely caused by the mechanisms responsible for the cloud formation (Elmegreen & Falgarone 1996).

At small scales, in the gravity-dominated regime, the self-similar picture is also expected to break down. No break point from self-similarity has yet been found in the

lower density gas, and Falgarone et al. (1998) report unresolved turbulent structures at scales as small as 0.02 pc from their study of the highest velocity gas in the Taurus molecular cloud (also Pety & Falgarone 2003). For the dense star-forming gas, on the other hand, Larson (1995) has inferred a break down of the self-similar behavior in the form of a discontinuity in the slope of the surface density of companions for young stars in Taurus. This break point divides the binary regime from the clustering regime, and it occurs approximately at a radius of 0.04 pc, which coincides with the Jeans length of the cloud. Such coincidence suggests that for scales smaller than this length, thermal pressure provides the dominant support against gravity, whereas for larger scales, turbulent and magnetic pressures are important (Larson 1995). Follow-up work by Simon (1997) shows similar break points in the density of stellar companions for Ophiuchus and the Orion Trapezium, although the scale-size of the break point does not follow the expected Jeans mass. A larger value for the break point in the self-similar behavior of Taurus has been proposed by Blitz & Williams (1997) based on ^{13}CO observations, although optical depth effects and molecular freeze-out (see Section 4.2) may have affected this estimate.

There is further evidence for a change in the structure of dark clouds at small scales. As mentioned above, the clump mass spectrum found from large-scale CO observations is relatively flat and follows a power law of the form $dN/dM \sim M^{-\alpha}$ with $\alpha =1.4$ to 1.8. The mass spectrum of millimeter/submillimeter dust continuum peaks, on the other hand, presents a steeper slope of $\alpha = 2.0$ to 2.5 for masses larger than about 1 $M_{\odot}$ (Motte, André & Neri 1998, Testi & Sargent 1998, Johnstone et al. 2000, 2001). This spectrum, which at least for the case of Ophiuchus flattens to about $\alpha = 1.5$ for lower masses (Motte, André & Neri 1998, Johnstone et al. 2000), mimics the shape of the initial mass function (IMF) of stars (Salpeter 1955, Miller & Scalo 1979) in contrast with the clump mass spectrum. Such similarity to the IMF suggests that stellar masses may be determined by the same process that fragments the molecular gas at the smallest scales.

The above discontinuity in the slope α still needs confirmation with a single observational technique, as each side of the break point has been observed with a different tracer (CO for large scales and millimeter/submillimeter continuum for small scales). If confirmed, the discontinuity will suggest a change in the physics of the cloud gas at the tenth of a parsec scale, and this can provide the basis for an empirical description of the different levels of cloud structure. Williams, Blitz & McKee (2000) have recently proposed one such categorization of structure in terms of clouds, clumps, and cores, with clumps being defined (as above) by their velocity coherence, and cores being defined as gravitationally bound, single-peaked regions out of which individual stars (or simple stellar systems) form. Alternative definitions have already been proposed (e.g., Goldsmith 1987, Myers 1995), and it is also possible that any description of cloud structure using only a few elements is too simple to capture the continuous properties of cloud gas (Rodríguez 2005). Still, the need to name and characterize the different levels in the hierarchical structure of clouds makes it necessary to have a well-accepted terminology, and the categorization by Williams, Blitz & McKee (2000) matches the spirit of current usage. Thus, using this convention, we present in **Table 1** a summary of the main physical parameters

of clouds, clumps, and cores. We stress that these units are still loosely defined and that their properties may be sensitive to the tracer used in the measurement and can vary with cloud. Future improvements in our understanding of cloud chemistry and structure will help further refine the above description.

2.7. Magnetic Field

The magnetic field of a cloud is probably its most difficult property to measure. The line-of-sight strength of the field can only be directly determined observing the Zeeman splitting of line transitions, and its plane of the sky direction can be estimated via polarization measurements of background stars, dust emission, or spectral lines. All these measurements require observations that combine stability and high signal to noise, and are therefore difficult and time consuming (see Heiles et al. 1993 for an in-depth review of observational techniques of magnetic field measurements). Although the magnetic field only acts directly on charged particles (electrons, ions, and charged dust grains), its presence can be felt by the neutral material through collisions. Under most dark cloud conditions, this ion-neutral coupling is highly efficient and, except for the densest regions, the field is expected to be frozen to the gas [see McKee et al. (1993) for a review of basic magnetic field theory]. Because of this, the ability of the magnetic field to counteract the action of self-gravity can be critical to the equilibrium balance of dark clouds.

The most straightforward way to map the large-scale orientation of the magnetic field in a cloud is to measure the polarization of light from background stars, which results from the dichroic extinction by aligned, elongated dust grains (Davis & Greenstein 1951). Large-scale maps of polarization for the Taurus cloud have been presented by Moneti et al. (1984) and Heyer et al. (1987). Goodman et al. (1990) have produced maps of the optical polarization for Perseus, Taurus, and Ophiuchus using a combination of their own measurements with previous data. From these maps, they find that in Taurus and Ophiuchus the pattern of polarization is highly regular over scales of about 10 pc, whereas the Perseus measurements seem to suffer from the superposition of two components along the line of sight. In Taurus and Ophiuchus, the large-scale filaments are neither completely parallel nor completely perpendicular to the global polarization pattern, suggesting that the magnetic field does not dominate the cloud structure on large scales (Goodman et al. 1990). Optical polarization data from other clouds offer a mixed picture. Clouds generally present fields with a well-defined mean direction but significant dispersion (Myers & Goodman 1991), and cases where the field is parallel or perpendicular to a filament exist (e.g., the long filamentary Musca cloud presents an ordered field perpendicular to the long axis of the filament; see Pereyra & Magalhães 2004).

Optical polarization measurements are necessarily limited to the low-extinction parts of a cloud, so the background stars are still bright enough to have their polarization measured. IR polarization data could, in principle, sample more opaque regions and therefore provide a deeper view of the inner magnetic field. Unfortunately, this seems not to be always the case. For the Taurus cloud, for example, there is evidence that the dust loses its polarizing power at depths larger than about $A_V = 1.3$, so IR

polarization measurements offer little improvement over optical data in this region (Goodman et al. 1995, Arce et al. 1998). This loss of polarizing power probably results from a combination of a change in the alignment properties of grains and a change in their optical properties because of coagulation and mantle growth, although the exact mechanism is not yet well understood (Lazarian, Goodman & Myers 1997, Whittet et al. 2001).

Better sampling of the innermost cloud regions is expected from polarization measurements of the millimeter/submillimeter emission from dust, although they also suffer often from drops in polarizing power toward the densest areas (Matthews, Wilson & Fiege 2001). Because of limitations owing to sensitivity and spatial filtering, large-scale studies of the dust polarization have concentrated on the brightest objects like the Orion filament (Matthews & Wilson 2000, Houde et al. 2004) instead of the more nearby and colder dark clouds (see Section 3.4 for submillimeter-polarization studies of dense cores). As in the case of the optical/IR polarization measurements, the limited submillimeter measurements do not show a very strong correlation between the magnetic field direction and the mass distribution in the clouds (e.g., Houde et al. 2004).

Zeeman effect observations of dark clouds provide an estimate of the strength of the (line-of-sight component of the) magnetic field. The high signal to noise required by these measurements and the low spatial resolution achieved, because of the low frequency of the transitions, means that no large-scale maps of Zeeman effect measurements are currently available. Observations are commonly restricted to single pointings, which offer only a limited sampling of the magnetic field strength in clouds. In addition, and owing to the need for strong emission, the pointings tend to be selected toward the densest regions. Still, coming up with meaningful detections is challenging, and the OH Zeeman observations of dark clouds by Crutcher et al. (1993) produced one clear detection out of 12 positions observed (mostly in Taurus and Ophiuchus). These data, together with the observations of Troland et al. (1996) suggest typical magnetic field strengths of order of 10 μG or less.

A main issue for the studies of the magnetic field strength in cloud gas is the importance of the field in the dynamics and balance of the cloud. A convenient parameter to characterize this importance is the mass-to-flux ratio normalized to the critical value $\alpha G^{1/2}$, where G is the gravitational constant and $\alpha \sim 0.13$ (see McKee et al. 1993 for a full discussion and equations). If the observed mass-to-flux ratio exceeds the critical value, the cloud is said to be supercritical and the magnetic field cannot prevent collapse. If the ratio is lower than the critical value, the cloud is called subcritical and gravity is stabilized by the magnetic field. A detailed compilation and analysis of the currently available data on magnetic field strength in molecular clouds has been presented by Crutcher (1999), and an update of this work appears in the review by Heiles & Crutcher (2005). According to this analysis, the magnetic field strength is just at the level of being critical, i.e., at the boundary between being dynamically important and not. Even in this best-to-date analysis, there are important caveats owing to the large number of nondetections and the need to correct geometrically the mass-to-flux ratio (multiplying by two in case of a sphere or by three in case of a sheet; see Bourke et al. 2001 and Heiles & Crutcher 2005). The values, in addition,

are likely more representative of the densest regions than of the extended cloud gas although chemical effects may further complicate the interpretation (Section 4.2). Thus, despite the enormous observational effort, the dynamical importance of the magnetic field in clouds, especially at the large scales, remains elusive. The current best guess is that the magnetic field contributes in a non-negligible way to the energy balance of molecular clouds. Whether it is a dominant player or a second order effect cannot be decided yet, and because of this, our understanding of the global equilibrium of dark clouds is still incomplete.

2.8. Equilibrium State and Star Formation

The equilibrium state of dark clouds and the way they collapse under gravity to form stars is probably the most controversial issue related to their nature. The uncertainties in the magnetic field strength and the importance of the turbulent motions, together with a possible revision of the lifetimes of the molecular gas (e.g., Hartmann, Ballesteros-Paredes & Bergin 2001), have resulted in two opposing views of the global state of clouds. Briefly, one view holds that clouds are close to equilibrium and that their evolution toward star formation is approximately quasi-static. The other view defends that clouds are dynamic objects that evolve and form stars in a crossing time. The limited space of this review cannot give justice to the number of issues involved in this controversy or to the detailed position of each camp, which consists of a number of researchers working often independently. Here we will simply review the main contentious points and mention a number of relevant references as an introduction to the topic. We refer the reader to the original papers and the reviews mentioned below for an in-depth view of the controversy.

The quasi-static view holds that clouds are objects close to equilibrium, owing to their relatively long lives (at least 10 Myr according to the recent estimate by Mouschovias, Tassis & Kunz 2006; see also Blitz & Shu 1980) and their being gravitationally bound and close to virialized (e.g., Larson 1981, McKee 1999). In this view, the equilibrium against self-gravity is provided by the magnetic field, which has a twofold contribution toward stability. If the static component of the magnetic field is strong enough to make the cloud subcritical, gravitational forces cannot overcome magnetic forces as long as the field remains frozen into the matter (Mestel & Spitzer 1956, Nakano & Nakamura 1978). Hydromagnetic waves, in addition, can provide additional support and contribute to the supersonic motions observed in molecular clouds (Arons & Max 1975, Gammie & Ostriker 1996). In this magnetically dominated picture, molecular clouds can only evolve under gravity and form stars through the process of "ambipolar diffusion," by which neutrals drift past the ions and the magnetic field, which remain frozen to each other. Through the action of ambipolar diffusion, cores of dense gas form by gravitational contraction out of the initially subcritical medium. When these cores have accumulated enough mass, they become supercritical and collapse to form stars (Mestel & Spitzer 1956; Shu, Adams & Lizano 1987; Mouschovias & Ciolek 1999). Under typical cloud conditions, ambipolar diffusion is slow (several cloud dynamical times, see Section 4.3.2), and this slowness makes cloud evolution prior to star formation occur quasi-staticly. It also makes star

formation a rather inefficient process, in agreement with the low rate of stellar birth observed in the Galaxy (Zuckerman & Evans 1974).

The more recent and opposite view of cloud evolution and star formation emphasizes the role of supersonic turbulence and lack of equilibrium. Numerical simulations have shown that magnetic turbulence decays in about a dynamical time (Mac Low et al. 1998; Stone, Ostriker & Gammie 1998; Padoan & Nordlund 1999), so hydromagnetic waves cannot provide support against gravity without a source of continuous replenishment. If in addition fields are weak enough so that molecular clouds are supercritical (Nakano 1998), cloud evolution and star formation becomes a fast process that occurs in a crossing time (Elmegreen 2000). In this picture, clouds form from convergent flows, evolve, and dissipate rapidly, without ever reaching a state of equilibrium, and with a typical molecular cloud lifetime of 3–5 Myr (Ballesteros-Paredes, Vázquez-Semadeni & Scalo 1999; Hartmann, Ballesteros-Paredes & Bergin 2001; Hartmann 2003; Vázquez-Semadeni, Ballesteros-Paredes & Klessen 2003). Molecular clouds are defined observationally by the detection of CO emission (as opposed to H_2 emission) and this lifetime refers to the age of the CO emitting cloud, which is associated with star formation. Chemical models suggest that H_2 formation is a prerequisite to CO formation (Bergin et al. 2004), and lifetime estimates do not include any earlier phase when gas is predominantly molecular (e.g., H_2) but CO has not formed in sufficient quantity for detectable emission. Factors such as ram pressure, molecule and dust shielding, and gas-grain physics influence the timescales for both H_2 and CO formation (Koyama & Inutsuka 2000, Bergin et al. 2004). But in any case, it is clear that substantial evolution ($\sim 10 - 20$ Myr) occurs in a pre-CO phase where the cold HI and H_2 would be difficult to detect (Bergin et al. 2004). Formation of cloud structure in this scenario is regulated by the stochastic action of turbulence, which produces strong density perturbations through its fluctuating velocity field. Regions of dense gas form at the stagnation point of two convergent flows (Padoan et al. 2001), although such a transient structure often disperses when the flows fade. If the initial compression is strong enough, it may decouple from the medium and produce a dense core that subsequently collapses to form stars. This process of creating structure through the interplay between gravity and turbulence is often referred to as gravoturbulent fragmentation (e.g., Klessen & Ballesteros-Paredes 2004) and lies at the heart of the dynamic picture of star formation (see the reviews by Larson 2003, Mac Low & Klessen 2004, and Ballesteros-Paredes et al. 2007).

The controversy between the fast and slow modes of cloud evolution and star formation is still ongoing and far from settled. Attempts to determine cloud lifetimes using stellar ages, for example, have not only failed to clarify the issue but have led to their own controversy (e.g., Palla & Stahler 2002, Hartmann 2003). Chemical analysis of the gas can also provide an estimate of cloud timescales. Observations of cloud cores, for example, suggest compositions that are far from equilibrium and ages that are $<3 \times 10^5$ years (e.g., Pratap et al. 1997, van Dishoeck & Blake 1998), although this chemical age might not reflect the true cloud age but rather refer to the last time the chemistry was reset by some dynamical event. Studies of cold HI in dark clouds, on the other hand, suggest longer timescales $>3 \times 10^6$ years (Goldsmith & Li 2005). Measurements of the magnetic field, as mentioned before, remain ambiguous

because the data populate the boundary between the critical and subcritical regimes (Crutcher 1999), and this is often interpreted as proof of the magnetic field being dominant or a minor player.

The above summary of the current controversy illustrates how our understanding of dark cloud physics is still limited and far from complete. The observations and theoretical work carried out over the past decade have clearly revitalized the field of cloud studies and challenged many ideas previously assumed correct. Unfortunately, they have not yet achieved a consensus view of how clouds form, evolve to form stars, and finally disperse. It is therefore a challenge left for the next generation of cloud studies to explain the diversity of observations and to develop a global view of clouds, from the large, tens-of-parsecs scale to the tenths-of-parsec size of the dense cores, to which we now will turn our attention.

3. PHYSICS OF PRESTELLAR MOLECULAR CORES

Dense cores are localized density enhancements of the cloud material that have been recognized for more than 20 years as the likely sites of low-mass star formation in nearby dark clouds like Taurus and Perseus. Initial core studies, based on the optical inspection of the Palomar plates together with molecular (especially NH_3) observations, showed that dense cores have typical sizes of 0.1 pc and contain a few solar masses of subsonic material at temperatures around 10 K and average densities of a few 10^4 cm^{-3} (Myers & Benson 1983, Benson & Myers 1989). The correlation of dense core positions with the location of highly embedded young stellar objects (YSOs) detected with the IRAS Far-Infrared satellite soon provided the proof that some dense cores are currently forming stars or have done so very recently (Beichman et al. 1986). The presence of an embedded YSO has also led to the classification of cores in two groups: starless and star-containing. Strictly speaking, the distinction between the groups is only based on the threshold for detection of an embedded YSO with current instrumentation, which was until recently of the order of 0.1 $L_\odot$ for nearby clouds like Taurus (Myers et al. 1987). The increase in the sensitivity of IR observations brought by *Spitzer* has led to the discovery of a number of so-called very low-luminosity objects (VeLLOs) in a few previously thought starless cores, forcing a revision of the core classification (e.g., L1014; see Young et al. 2004). Still, the distinction between starless and star-containing cores seems a fundamental one, as it likely represents the separation between the prestellar and poststellar phases of core contraction. The study of starless cores, therefore, offers the best opportunity to determine the initial conditions of low-mass stellar birth.

Dark globules (often called Bok globules or Barnard objects) are classically defined by their optical appearance as small, roundish, and dark nebulosities (Bok & Reilly 1947). They constitute a less homogeneous class than the dense cores of dark clouds, as they span sizes up to about 1 pc and masses of up to almost 10^3 $M_\odot$, and have lower average densities (Bok 1977). A number of small globules, however, share many characteristics with the dense cores and are also the formation sites of individual low-mass stars (Clemens & Barvainis 1988, Yun & Clemens 1990). These dense globules may have a similar formation mechanism as the dense cores, with the difference

that globules do not lie embedded in a molecular cloud because they have been exposed by an external event (such as ionization from a nearby O star; Reipurth 1983). Like some dense cores, some globules seem starless and centrally concentrated, and probably represent a phase prior to gravitational collapse. As we will see below, their isolated nature provides an additional advantage when studying the internal structure of prestellar objects (Alves, Lada & Lada 2001).

The study of dense cores and globules prior to star formation has progressed enormously during the past decade. Earlier work lacked the angular resolution needed to study their internal structure, and it therefore concentrated on global properties like total masses and average densities (e.g., Clemens & Barvainis 1988, Benson & Myers 1989). The progressive increase in resolution and sensitivity of radio and IR observations has finally allowed a detailed view of their interior. Through a combination of techniques that trace the gas and dust components, a new understanding of their internal structure has started to emerge. Crucial to this understanding has been the realization that dense cores and globules, despite their apparent simplicity, have a rather complex chemical composition that is responsible for previous contradictions between observations made with different tracers. In this section we review some of the recent results concerning the physical structure of starless cores and globules, and the following section does the same for their chemical properties. For the sake of economy, we refer to both cores and globules simply as cores, and we only make an explicit distinction between the two when necessary. We also use the term starless in a broad sense that includes what in the literature is sometimes referred to as prestellar.

3.1. Density

The density structure of prestellar cores is typically estimated through the analysis of dust emission or absorption. Three main techniques have been used so far: (*a*) near-IR extinction mapping of background starlight, (*b*) mapping of millimeter/submillimeter dust continuum emission, and (*c*) mapping of dust absorption against the bright Galactic mid-IR background emission. Each technique uses dust observations to derive a parameter that is proportional to the gas column density, and then fits this parameter with a model density profile that assumes some simple geometry (usually spherical). **Figure 3** shows a summary of how each technique works, including maps of representative cores (B68, L1544, and ρ Oph D), the main equations used in the analysis, and the radial profiles of the dust-derived parameter to be fit with the density model.

Because of their different assumptions, the above techniques are sensitive in different ways to the properties of the dust and to the variation of these properties inside the core. Uncertainties in the dust parameters propagate in different manners and affect differently the final density determination of each technique. The near-IR extinction method, for example, is independent of the dust temperature, but depends on the reddening law (using $r_v^{H,K}$ to convert A_K into A_V) and on the correlation between A_V and the gas column density, both of which may be variable (see Rieke & Lebofsky 1985 and Bohlin et al. 1978 for typical interstellar medium values). The millimeter/submillimeter dust continuum emission method, on the other
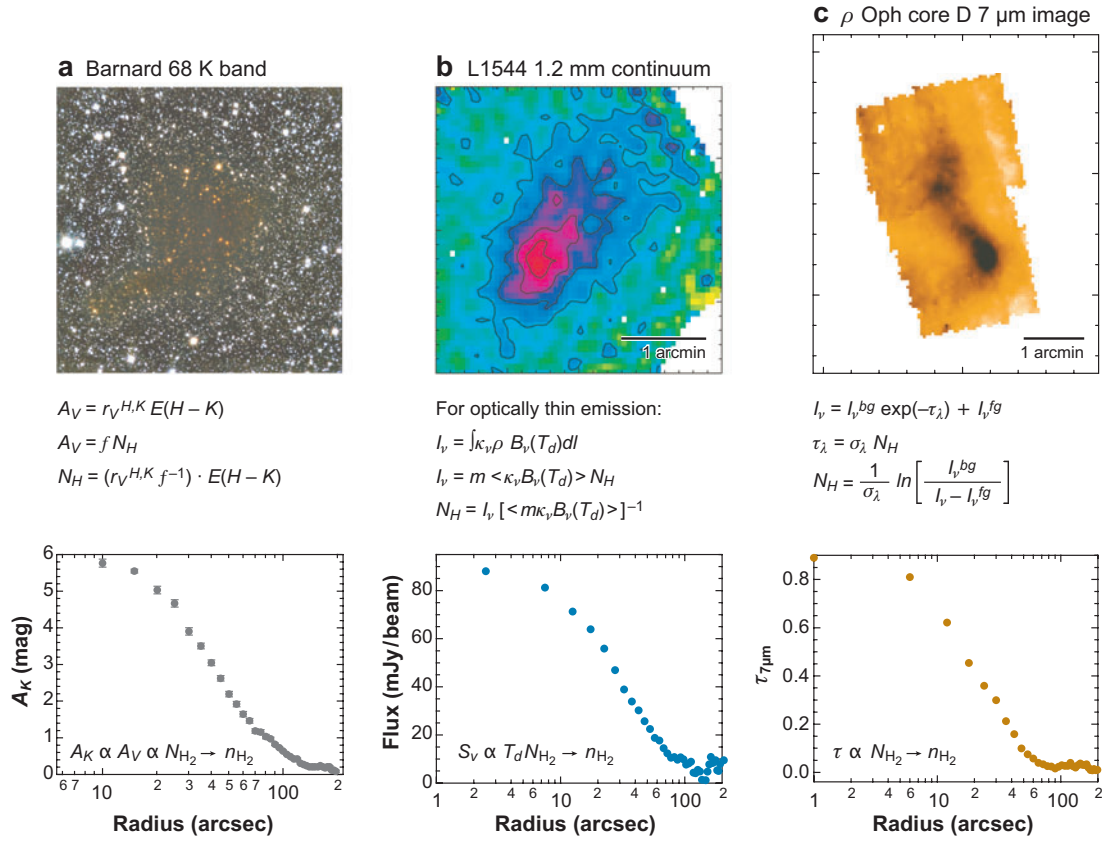
c ρ Oph core D 7 μm image

a Barnard 68 K band

b L1544 1.2 mm continuum

$A_V = r_V{}^{H,K} E(H-K)$

$A_V = f N_H$

$N_H = (r_V{}^{H,K} f^{-1}) \cdot E(H-K)$

For optically thin emission:

$I_\nu = \int \kappa_\nu \rho\, B_\nu(T_d) dl$

$I_\nu = m <\kappa_\nu B_\nu(T_d)> N_H$

$N_H = I_\nu [<m\kappa_\nu B_\nu(T_d)>]^{-1}$

$I_\nu = I_\nu{}^{bg} \exp(-\tau_\lambda) + I_\nu{}^{fg}$

$\tau_\lambda = \sigma_\lambda N_H$

$N_H = \dfrac{1}{\sigma_\lambda} ln\left[\dfrac{I_\nu{}^{bg}}{I_\nu - I_\nu{}^{fg}}\right]$

$A_K \propto A_V \propto N_{H_2} \rightarrow n_{H_2}$

$S_\nu \propto T_d N_{H_2} \rightarrow n_{H_2}$

$\tau \propto N_{H_2} \rightarrow n_{H_2}$

Figure 3

Figure illustrating the various methods used to determine the column and volume density of starless molecular cores. (*a*) K-band image of Barnard 68 and plot of the derived A_K with 10 arcsec resolution as a function of core radius [taken from Alves, Lada & Lada (2001)] with A_K versus radius provided by C. Román-Zúñiga. In this method the measured quantity is the H–K excess, which is related to A_V by the extinction law, parameterized by $r_v{}^{H,K}$. A_V is correlated to the hydrogen column from UV line measurements, parameterized by f (Bohlin et al. 1978, Rachford et al. 2002). (*b*) 1.2-mm dust continuum emission map and flux versus radius for L1544 (taken from Ward-Thompson, Motte & André 1999 and Tafalla et al. 2002). κ_ν is the dust opacity per unit gas mass, ρ is the dust density, and m the hydrogen mass (corrected for He). (*c*) 7-μm ISOCAM image and opacity versus radius for ρ Oph D (taken from Bacmann et al. 2000). At 7 μm the emission from polycyclic aromatic hydrocarbons provides a bright background, and the dense core appears in absorption. In this method the absorbing opacity is related to the hydrogen column via the dust absorption cross section, σ_λ.

hand, depends almost linearly on the dust temperature and on the value of the dust emissivity (κ_ν), two parameters that are known to vary systematically as a function of core depth (see Section 3.2.1 for more details). The mid-IR absorption method is also subject to uncertainties. It is sensitive to fluctuations in the emission from polycyclic aromatic hydrocarbons, which provide the bright background against which

the core is observed. It also depends on the somewhat uncertain relation between the absorbing opacity and the hydrogen column density (see Weingartner & Draine 2001 and Ragan et al. 2006 for further details). Given the restricted use of each of these methods (owing to their difficulty and data requirements), no systematic intercomparison between them has been carried out so far. As shown below, the methods agree in the qualitative characteristics of the density profiles, but a quantitative comparison of the inferred densities is still seriously needed. Without this, we can only guess the relative uncertainties of our density determination; current wisdom suggests that they are in the factor-of-2 range.

A main characteristic of the density profiles derived with the above techniques is that they require a central flattening. Pioneering work by Ward-Thompson et al. (1994) showed that the radial profiles of submillimeter continuum emission for a number of cores could not be fitted using single power-law density distributions (assuming a constant dust temperature). At least two power laws were needed to fit the data, and the inner power law was always flatter than the outer one, which was usually close to r^{-2}. Follow-up work with higher sensitivity has confirmed these early results for an increasing number of objects, and it has shown that as a rule, the density gradient of a core is flatter than r^{-1} within radii smaller than 2500–5000 AU, and that the typical central density of a core is 10^5–10^6 cm^{-3} (André, Ward-Thompson & Motte 1996; Ward-Thompson, Motte & André 1999). Although a dust temperature drop toward the core center is expected from thermal equilibrium considerations (Evans et al. 2001), the effect seems too weak to explain alone the flattening found in the continuum data. Observations using extinction techniques, which are insensitive to temperature, also find that a central flattening of the density profile is needed to fit the data. Bacmann et al. (2000), for example, have modeled mid-IR (7 μm) absorption profiles from a sample of nearby starless cores observed with ISOCAM, and they have found that a decrease in the slope of the density distribution is required to fit the emission in the central 4000–8000 AU. Alves, Lada & Lada (2001) have mapped in detail the near-IR extinction from the B68 globule and achieved an almost perfect fit with an equilibrium isothermal (Bonnor-Ebert) density profile that has a central flattening within ∼5000 AU. Density profiles comparable to those inferred from observations are shown in **Figure 4**.

A number of density laws with central flattening have been used to fit the observations of dense cores. The dual power law used initially by Ward-Thompson et al. (1994) is illustrative of the need for inner flattening, but presents an unphysical discontinuity in the derivative that results in a pressure jump. A simple alternative is the softened power laws used by Tafalla et al. (2002), and a more physical model is the truncated isothermal (Bonnor-Ebert, BE) sphere (Ebert 1955, Bonnor 1956), that often (but not always) provides a good fit to the data. Examples of good BE fits include those to the extinction profiles of a number of Bok globules (Alves, Lada & Lada 2001, Kandori et al. 2005) and dense cores (Bacmann et al. 2000). Other physical models, on the other hand, seem to be ruled out by these observations. The logotropic density profile of McLaughlin & Pudritz (1996) is too flat at large radii (r^{-1}) to fit most cores (Bacmann et al. 2000), whereas the Plummer-like profile (Whitworth & Ward-Thompson 2001) seems asymptotically too steep (r^{-4}). Less
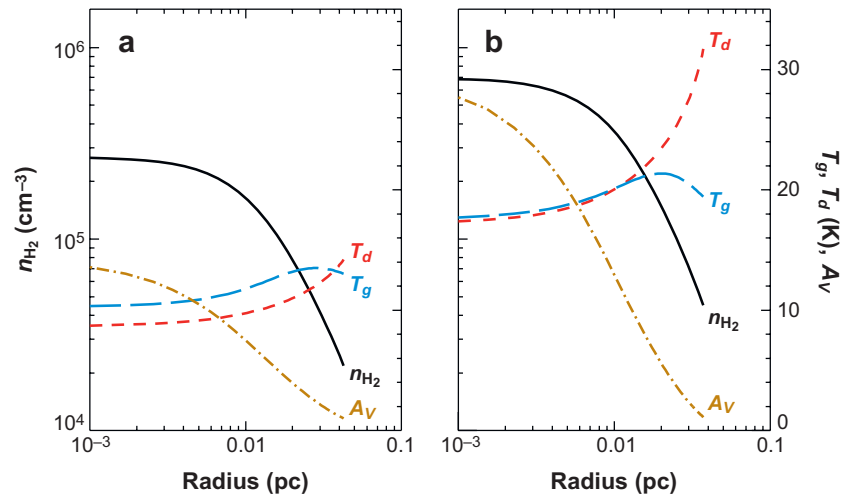
Figure 4

(*a*) Molecular hydrogen density, n_{H_2}, gas (T_g) and dust (T_d) temperatures, and visual extinction (A_V) as a function of radius for a marginally stable spherical cloud with $M = 1\,M_\odot$ exposed to the standard interstellar radiation field ($G_0 = 1$). (*b*) Same as (*a*) but for a marginally stable cloud ($M = 1.6\,M_\odot$) bounded by an external pressure ($p_{ext} = 10^6\,\mathrm{K\,cm^{-3}}$) and illuminated by an enhanced radiation field ($G_0 = 10$). Figure taken from Galli, Walmsley & Gonçalves (2002).

clear is the situation of magnetic field–dominated models. These models naturally produce equilibrium configurations with flattened density profiles and approximately r^{-2} power-law behavior at large radius (e.g., Mouschovias 1976; Tomisaka, Ikeuchi & Nakamura 1988; Lizano & Shu 1989). Bacmann et al. (2000) find that some of these configurations provide adequate fits to their data, but that they require magnetic fields of the order of 50–150 μG, significantly larger than commonly observed (Section 3.4). They also predict oblate geometries, which seems to contradict some observations (Myers et al. 1991).

The high quality of some BE fits raises the question of whether cores are truly isothermal spheres solely supported by thermal pressure and confined by an outer medium. Several lines of evidence suggest that although thermal pressure is an important ingredient in core structure, it is not the only one, and that cores are more complex entities than simple BE spheres. In the first place, cores are seldom spherical, but they appear in the sky as elliptical objects with axial ratios typically of 2:1 (Myers et al. 1991). Whether cores are prolate, oblate, or triaxial is still a matter of some debate (Myers et al. 1991; Ryden 1996; Jones, Basu & Dubinski 2001), but the lack of spherical symmetry already suggests either the presence of a nonsymmetrical force component or the lack of perfect equilibrium. In addition, the observed density contrast between the core center and its edge often exceeds the maximum value of ≈14 allowed for stable BE spheres (Bacmann et al. 2000, Evans et al. 2001), and it seems unlikely that such an unstable configuration can be realized in nature if thermal pressure is the only balancing force. Finally, the pressure required by the BE fits

usually exceed the thermal (plus subsonic nonthermal) pressure available from the gas by a factor of a few, again indicating the presence of an additional force component or the lack of equilibrium (Tafalla et al. 2004; Kirk, Ward-Thompson & André 2005).

The BE-like profiles found when fitting observations must therefore result from more complex physics than just thermal hydrostatics. Indeed, Myers (2005) and Kandori et al. (2005) have shown that these profiles can be reproduced with a variety of geometries and even under early conditions of gravitational collapse. Even models of supersonic turbulence can produce density condensations that have in projection the appearance of BE profiles (Ballesteros-Paredes, Klessen & Vázquez-Semadeni 2003), but their expected velocity structure is inconsistent with the prevalence of subsonic cores in dark clouds like Taurus (e.g., Jijina, Myers & Adams 1999, Tafalla et al., in preparation). The ultimate origin of the observed core density profiles remains therefore unexplained.

3.2. Temperature

The kinetic temperature of the dust and the gas components in a core is regulated by the equilibrium between heating and cooling. At typical core densities ($>10^4$ cm^{-3}), the gas and dust start to couple thermally via collisions (e.g., Goldsmith & Langer 1978, Burke & Hollenbach 1983), and the two temperatures are expected to converge; whether they equalize or not depends in part on the exact density of the core and on the strength of the external radiation field (Galli, Walmsley & Goncalves 2002). In this and the next sections we discuss recent progress in the determination of the dust and gas temperatures of cores. As the two temperatures are determined using different observational techniques and are therefore subject to different uncertainties, we separate their discussion. We start with the dust.

3.2.1. Dust temperature. The dust temperature is physically determined by the balance between the heating by the interstellar radiation field (ISRF) and the cooling by thermal radiation from the grains in the far-IR (Mathis, Mezger & Panagia 1983). To estimate this temperature observationally, color measurements of the dust in the submillimeter or far-IR are commonly used, sometimes complemented with near-IR extinction measurements. A major uncertainty in this work is our limited understanding of the optical properties of the dust and, in particular, the value of the dust emissivity and how it changes as a function of density. Theoretical models of dust evolution predict that as the density increases, the dust grains become coated with ice and coagulate to form fluffy aggregates, changing their emissivity in the process (Ossenkopf & Henning 1994). Determining dust temperatures from observations therefore implies simultaneously resolving for its optical properties, in particular the emissivity (κ), and its wavelength dependence (commonly parametrized as ν^β).

Large-scale studies of dust temperature show that the grains in starless cores are colder than in the surrounding lower-density medium, as expected from the attenuation of the ISRF deep inside the cloud. From ISO far-IR (170 and 200 μm) observations toward the vicinity of a number of dense cores, Ward-Thompson, André & Kirk (2002) found a prevalence of flat or decreasing temperature gradients with

cloud temperatures of 15–20 K and core values of 10–12 K. Because of the 1-arcmin resolution of these observations (0.04 pc at the distance of Taurus), the core value represents only an average temperature over the densest gas. Also using low-resolution ISO data and a similar analysis, Tóth et al. 2004 and del Burgo & Laureijs (2005) have derived inward temperature gradients that reach central values of ≈12 K for a number of Taurus cores, whereas for the denser L183 core a value close to 8 K has been measured (Lehtinen et al. 2003, Pagani et al. 2003). These temperature estimates, however, ignore the effects of grain evolution and assume a constant dust emissivity, while observations are beginning to show that the emissivity does in fact vary. Far-IR observations of a filament in Taurus by the PRONAOS balloon-borne experiment suggest that at the highest densities, the population of smallest grains disappears and the submillimeter emissivity increases by a factor of about 3, as expected by models of dust coagulation into fluffy grains (Stepnik et al. 2003). These observations also suggest inner dust temperatures around 12 K, although the 3-arcmin resolution sets an important limitation.

The trend of decreasing dust temperature with depth observed in the large-scale maps is expected to continue inside the dense cores, but the exact shape of the resulting gradient is still a matter of some uncertainty. Initial models by Evans et al. (2001) and Zucconi, Walmsley & Galli (2001) suggested sharp core edge-to-center drops in temperature of about a factor of two (an example is provided in **Figure 4**). However, these models either assumed that cores are directly exposed to the ISRF (correct for Bok globules only) or use a simple attenuation law for cores that are embedded in clouds. André et al. (2003) and Stamatellos & Whitworth (2003) have argued that the effect of the surrounding cloud is to flatten the temperature gradient, so that at the center of an embedded core the gradient is less pronounced (see Stamatellos et al. 2004 or Goncalves, Galli & Walmsley 2004 for 2D and 3D radiative transfer models). Irrespective of the models, however, central dust temperatures close to 7–8 K are predicted for typical dense cores, with the exact value depending on the dust central density and the presence or not of a surrounding cloud.

From an observational point of view, possible gradients in the dust emissivity still limit our estimate of the temperature profiles. Kramer et al. (2003) have combined submillimeter emission and near-IR extinction data to study several starless cores in IC 5146. With an angular resolution of 30 arcsec, these researchers find that the dust temperature is typically 12 K and close to constant inside the cores, while the surrounding, lower extinction material has a higher value of about 20 K. They also find that the dust emissivity increases systematically by a factor of 4 between 20 K and 12 K, consistent with models of dust evolution (e.g., Ossenkopf & Henning 1994). Using similar technique and angular resolution, Bianchi et al. (2003) have also found an emissivity gradient in the B68 globule, together with an outer dust temperature of 14 ± 2 K and an inner temperature drop of a factor of 1.5. Schnee & Goodman (2005), on the other hand, have studied the submillimeter emission from TMC-1C with 14 arcsec resolution and found a central gradient in the submillimeter color. As illustrated in **Figure 5**, this color gradient can result from either a central temperature drop to about 7 K or a systematic change in the dust emissivity index (or both). Clearly more data and modeling are needed to characterize the existing
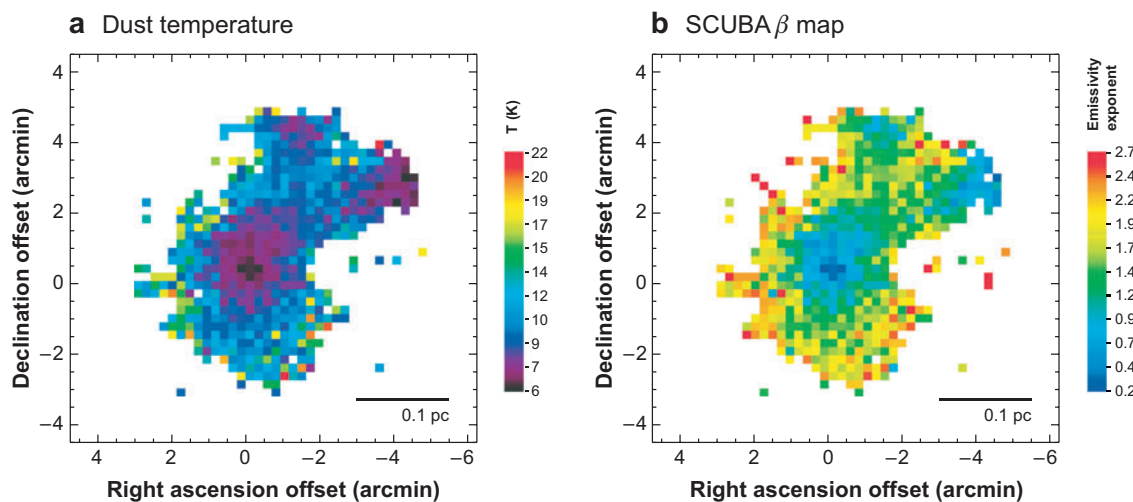
a Dust temperature

b SCUBA β map

Figure 5

(*a*) Map of dust temperature in TMC-1C derived from 450 and 850 μm SCUBA maps assuming dust emissivity index $\beta = 1.5$. (*b*) Map of dust emissivity index, β in TMC-1C assuming a constant temperature of 10 K. Taken from Schnee & Goodman (2005).

gradients in dust conditions inside dense cores. Future multiwavelength mapping in the far-IR with the *Herschel Space Observatory* (*Herschel*) offers the best hope to finally disentangle the changes in temperature and optical properties.

3.2.2. Gas temperature. Like the dust temperature, the temperature of the gas is determined by the balance between heating and cooling. For the lower density cloud gas, heating mostly occurs through ionization by cosmic rays, while the cooling is mainly due to line radiation from molecules, especially CO (Goldsmith & Langer 1978). At the high densities of cores (more than a few 10^4 cm^{-3}), gas-dust coupling via collisions becomes important, and this process will additionally heat or cool the gas depending on the difference between the gas and dust temperatures (Burke & Hollenbach 1983). Also at these densities, and at typical core temperatures, CO and other molecules start to disappear from the gas phase owing to their freeze-out onto the dust grains (Section 4.2), diminishing the ability of the gas to cool down via line radiation. The detailed study of thermal balance in dense cores by Goldsmith (2001) shows that the gas-dust coupling, together with the high efficiency of the dust radiative cooling, easily compensates the disappearance of molecular coolants and keeps the temperature of the gas deep inside the core at rather low values, comparable to those of the dust component. At the lower-density core edges, the gas and dust are thermally decoupled and the gas can become warmer than the dust due to photoelectric heating. The temperature difference between the two components depends on the strength of the external UV field (see **Figure 4**).

Keeping the gas cold and at a close-to-uniform temperature has important implications for the mechanical equilibrium of cores, as the gas component is the main

contributor to the thermal pressure. Galli, Walmsley & Goncalves (2002) have studied the equilibrium structure of a pressure-supported dense core with a realistic treatment of the gas and dust cooling. Although the resulting gas temperature distribution is not exactly constant, its gradient is shallow enough to require for stability a density profile that is very close to the BE solution (see **Figure 4**). Thus, if cores were supported by thermal pressure only, the BE model would be consistent with the internal thermodynamics.

To measure the temperature of the gas component in clouds and cores, the level excitation of simple molecules like CO and NH_3 is commonly used (Evans 1999). CO and its isotopologues have small dipole moments, so their lower energy levels thermalize at relatively low densities of the order of few 10^3 cm^{-3} (Spitzer 1978), typical of the extended gas in dark clouds. Temperatures derived using CO in regions with no star formation indicate gas temperatures of 10–15 K, with a possible increase toward the lower density gas near the cloud edges (Snell 1981). Temperatures for the denser gas in cores are better determined using the metastable inversion levels of ammonia (NH_3), which can be observed simultaneously at a wavelength of about 1.3 cm (Walmsley & Ungerechts 1983). NH_3, in addition, appears to rise in abundance in the densest ($n_{H_2} > 10^4$ cm^{-3}) regions (Section 4.2), so it tends to selectively trace dense core gas. Low angular resolution NH_3 observations of dense cores typically indicate gas temperatures of about 10 K with a rather narrow range of variation for clouds like Taurus, Perseus, and Ophiuchus (Myers 1983; Benson & Myers 1989; Jijina, Myers & Adams 1999). These low-resolution measurements represent core-wide averages of the temperature and are in reasonable agreement with the theoretical expectations mentioned before. Owing to the relatively low angular resolution of the NH_3 observations (caused by the low frequency of the transitions), few studies of the radial dependence of the gas temperature inside dense cores have been made. Tafalla et al. (2004) have studied the temperature profiles of two Taurus-Auriga starless cores, L1498 and L1517B, using NH_3 observations with a resolution of 40 arcsec (0.027 pc). In both cores, the temperature remains constant over the central 0.1 pc with a value of about 10 K. Higher resolution NH_3 observations of the denser starless core L1544 seem to indicate a decrease of the gas temperature toward the innermost parts of the core (Crapsi et al., in preparation). For the starless Bok globule B68, however, Bergin et al. (2006) have found an opposite effect. Although the inner core traced by NH_3 is at about 10 K, the surrounding layers, traced with CO isotopologues, are slightly cooler (7–8 K). This central warming may result from a weakening of the gas-dust coupling at the highest densities due to grain coagulation. Given this diversity of results, further observations of the temperature gradients inside dense cores are needed to clarify the origin of these significant, but relatively small (20%), temperature differences.

3.3. Velocity Structure

In contrast with the supersonic velocity fields characteristic of the clouds as a whole, dense cores have low-velocity internal motions. Starless cores in clouds like Taurus, Perseus, and Ophiuchus systematically present spectra of core-tracing species (e.g.,
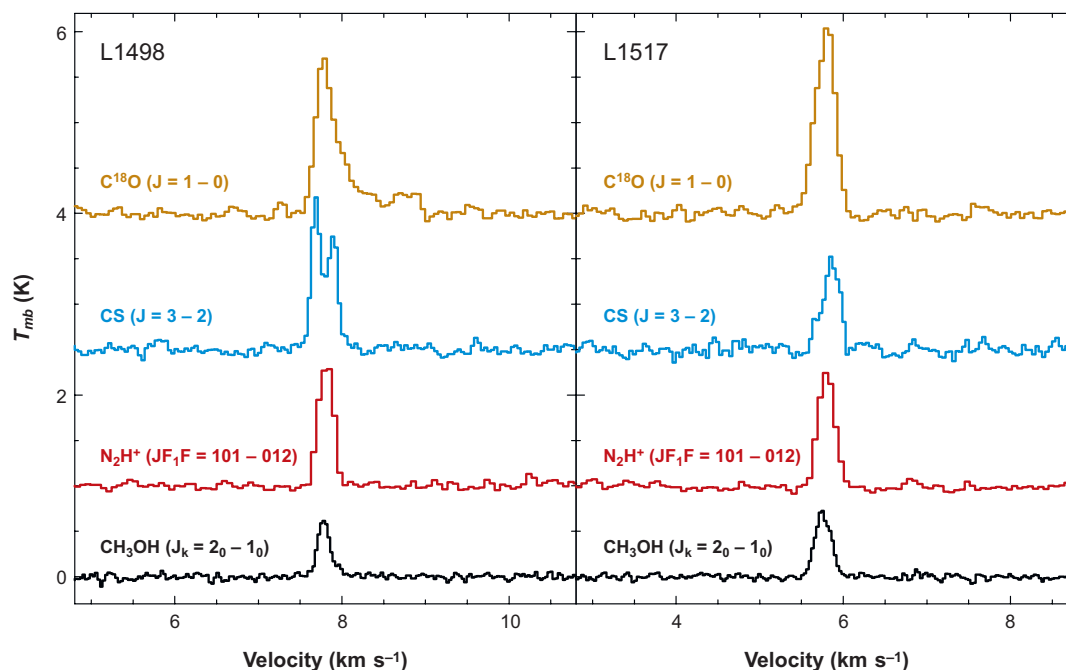
Figure 6

Sample spectra from the starless cores L1498 and L1517B in the Taurus-Auriga dark cloud illustrating the variety of shapes and intensities commonly observed. The $C^{18}O$ spectra trace both dense and low-density gas (owing to the low dipole moment of the molecule), and often present additional velocity components from unrelated gas that moves at velocities of the order of 1 km s^{-1} (red gas in L1498). The optically thick CS spectra are sensitive to the relative motions of the core and its envelope thanks to the presence of self-absorptions, which commonly indicate inward (L1498) or outward (L1517B) motions at the level of 0.1 km s^{-1}. The optically thin N_2H^+ and CH_3OH lines trace different regions of the core depending on their chemistry, and their narrow linewidths reveal the subsonic nature of the gas internal motions. Data from Tafalla et al. (2004, 2006).

NH_3) that have close-to-thermal linewidths, even when observed at low angular resolution (Myers 1983; Jijina, Myers & Adams 1999). This indicates that the gas motions inside the cores are subsonic, either in the form of random turbulence or as part of more systematic global patterns (**Figure 6**).

Despite the slow speeds involved, the internal motions of cores are generally complex; no single element is identified as dominant. The excess in linewidth over the thermal value has commonly been interpreted as resulting from turbulent motions, although as we show below, other velocity patterns like infall could contribute to the line broadening. Even in this interpretation, turbulent motions, by being subsonic, contribute less to the gas pressure than the thermal component, so they represent a minor contribution to the core support (Myers 1983, Goodman et al. 1998, Caselli et al. 2002a, Lada et al. 2003, Tafalla et al. 2004). Studying the spatial distribution of turbulent motions in cores, Goodman et al. (1998) have found that they deviate from

the linewidth-size relation seen at large scales (Section 2.5, Larson 1981). Instead, the nonthermal component of the NH_3 linewidth in a core is approximately constant inside a "coherence" radius of about 0.1 pc (see also Caselli et al. 2002a, Tafalla et al. 2004). This coherence radius is close to the 0.04-pc radius found to separate the binary and clustering regimes in Taurus and interpreted as the length-scale at which the cloud self-similar behavior breaks down (Section 2.5, Larson 1995). It is therefore tempting to suggest that the coherence radius is the scale at which turbulence loses its grip on cloud motions and allows the formation of thermally dominated cores.

A rotation component is expected in any object that forms by the gravitational contraction of Galactic material (Spitzer 1978). From the study of the spatial changes in the velocity centroid of lines, however, it has been known for some time that dark clouds as a whole are not rotating rapidly (Heiles & Katz 1976, Arquilla & Goldsmith 1986). Observations of dense cores and globules reveal a similar lack of fast rotation in the dense gas. Goodman et al. (1993) analyzed the rotation patterns of 43 dense cores as derived from observations of the NH_3 (1,1) line and estimated that the typical ratio between rotational and gravitational energies is only 0.02. These researchers also found no correlation between the rotational axis and the orientation of core elongation, which is again indicative of rotation being only a minor element in core support. From higher resolution N_2H^+ observations of an equivalent sample of cores, Caselli et al. (2002a) have derived similarly low values of the rotational energy and found that the point-to-point velocity gradients inside the cores are much more complex than expected for simple solid-body rotation. Rotation is therefore only one of the ingredients of core kinematics.

The slow rotation rate of dense cores is in fact remarkable. Arquilla & Goldsmith (1986) and Goodman et al. (1993) have shown that the specific angular momentum j in a core or a cloud scales with its radius R approximately as $R^{1.6}$. Clouds of 1-pc radius have typical j values around 10^{23} cm^2 s^{-1}, whereas typical cores (0.05-pc radius) have j values of about 10^{21} cm^2 s^{-1}. If this trend of decreasing j reflects the evolution of specific angular momentum as the cloud gas undergoes contraction, an efficient mechanism of angular momentum removal is required to reproduce the observations, and in particular, to explain the low j values of cores. Magnetic coupling between the contracting gas and the lower density environment has been classically favored as the mechanism for transferring angular momentum from a contracting core to its surroundings (Mestel & Spitzer 1956, Mouschovias & Paleologou 1979), although an alternative interpretation in terms of gravoturbulent fragmentation has recently been proposed (Jappsen & Klessen 2004). The low j value of cores is in fact comparable to or slightly larger than the value inferred for protostellar envelopes, T Tauri disks, and wide binaries, suggesting that the later phase of gravitational contraction of the core occurs with almost constant angular momentum (Bodenheimer 1995). Of course, a final phase of angular momentum redistribution via disk transport or tidal interactions between stars is still needed to explain the low specific angular momentum found in individual T Tauri stars (e.g., Shu, Adams & Lizano 1987; Bodenheimer 1995; Larson 2002).

Inward motions can also contribute to the dense core kinematics. They are inferred from the observation of optically thick, self-absorbed lines of species like CS,

H$_2$CO, or HCO$^+$, in which low-excitation foreground gas absorbs part of the background emission. In a core with inward motions, the foreground gas moves toward the background, so the absorbing material is red-shifted with respect to the emitting layers. The resulting spectrum is a self-absorbed profile with a red-shifted dip and a relatively brighter blue peak [see CS($J = 3 - 2$) in **Figure 6**], a pattern often called an infall asymmetry (Leung & Brown 1977, Myers et al. 1996). In a starless core, this spectral feature was first identified through observations of L1544, for which an average inward velocity of about 0.1 km s^{-1} was inferred (Myers et al. 1996, Tafalla et al. 1998, Williams et al. 1999, Caselli et al. 2002b). A follow-up single-pointing survey of 220 starless cores by Lee, Myers & Tafalla (1999) has found a statistically significant overabundance of inward motions with typical velocities of 0.05–0.1 km s^{-1}, indicating that subsonic contraction is a common feature of core kinematics (also Gregersen & Evans 2000). The spatial distribution of these motions is typically large, 0.05–0.15 pc, and comparable to the observed size of the cores (Tafalla et al. 1998, Lee, Myers & Tafalla 2001). Such a large extent could result either from the gravitational collapse of a core having a centrally condensed initial state (Myers 2005) or be associated with the process of core condensation (see Myers, Evans & Ohashi 2000 for a review).

Additional velocity patterns have been proposed to explain the observations of molecular lines in different cores. Lada et al. (2003) found an asymmetric velocity field with both inward and outward motions in the B68 globule, and they speculate it results from small amplitude pulsations of the core outer layers. Such a pattern seems in fact consistent with the close to BE density structure found in this object (Keto et al. 2006). Tafalla et al. (2004) proposed that residual internal motions in L1498 and L1517B may originate from asymmetric contraction, as the motions are correlated with asymmetries in the pattern of depletion of species like CO and CS. Finally, by comparing the velocity centroids of N$_2$H$^+$ and CO isotopologues in a sample of 42 cores, Walsh, Myers & Burton (2004) have concluded that the relative velocity between the dense cores and the ambient medium is low ($\leq$0.1 km s^{-1}). This implies that newly born stars are not expected to move appreciably from their natal cores.

3.4. Magnetic Field

Estimates of the magnetic field in starless cores are mainly obtained from Zeeman splitting measurements and from polarization observations of the millimeter/ submillimeter dust continuum. Zeeman measurements provide a direct estimate of the strength of the (line-of-sight component of the) magnetic field, B_{los}, but have the disadvantage of a low angular resolution and the use of tracers sensitive to molecular depletion, so they are prone to miss the densest part of the cores. From OH Zeeman measurements of the L1544 core with the Arecibo telescope, Crutcher & Troland (2000) estimated a line-of-sight strength of about 11 μG averaged over a beam of 3 arcmin (about 0.1 pc), in good agreement with the prediction from a previous model of ambipolar diffusion (Ciolek & Basu 2000). These observations, however, are more sensitive to the large-scale cloud gas than to the core material because of the the low dipole moment and the chemical distribution of the OH molecule in clouds

(Section 4.2). Zeeman measurements using tracers of dense gas have mostly produced negative results, like $B_{los} \leq 100$ μG in L1498 (CCS data, Levin et al. 2001) and $B_{los} \leq 15$ μG in TMC-1 (C$_4$H data, Turner & Heiles 2006). Shinnaga, Tsuboi & Kasuga (1999), however, have reported an estimate of 160 ± 42 μG in the young starless core L1521E from CCS observations.

Submillimeter polarization measurements provide a direct estimate of the orientation of the (plane-of-the-sky component of the) magnetic field. They can also be used to estimate indirectly the strength of the field by comparing the spatial dispersion of its orientation and the turbulence level of the gas (Chandrasekhar & Fermi 1953). As mentioned in Section 2.7, these measurements often lose sensitivity toward the brightest, highest density regions, where the polarization fraction drops with intensity (Matthews & Wilson 2000; Henning et al. 2001; Wolf, Launhardt & Henning 2003), which again makes the estimates more sensitive to the field in the outer parts of the cores. Because of the combination of weak submillimeter emission of the starless cores and a low polarization fraction (∼10%), these observations are challenging and have only been carried out in a reduced number of objects. For cores L1544, L183, and L43, Ward-Thompson et al. (2000) and Crutcher et al. (2004) have found polarization vectors that are fairly uniform but not aligned with the minor axis of the cores by about 30°, as would have been expected by ambipolar diffusion models (but see Basu 2000 for an alternative view if the cores are triaxial). From the dispersion of the polarization vectors and the turbulence level of the gas, these researchers estimate plane-of-the-sky intensities between 80 and 160 μG. Strictly speaking, these field intensities make the cores supercritical (i.e., with a magnetic field too weak to balance gravity). However, the inclusion of a geometrical correction factor moves the cores to the critical or slightly subcritical regime, suggesting that the field may be dynamically important (Crutcher et al. 2004). Lower field values of 10 and 30 μG have been estimated toward the cores L1498 and L1517B, respectively, indicating that these cores may be supercritical by factors of about two even after geometrical correction (Kirk, Ward-Thompson & Crutcher 2006).

As with the large-scale magnetic field measurements (Section 2.7), the observations of cores provide an ambiguous answer to the question of whether or not magnetic fields dominate the equilibrium of dense cores. Clearly more observations of both the Zeeman effect and the dust polarization are needed to clarify the role of magnetic fields in the process of core and star formation. The close to critical values observed so far, however, suggest that unless observations have been systematically biased in one or the other direction, cores appear to be close to the point of criticality to within a factor of about two. Explaining this apparent coincidence should therefore be a main requirement to any theory of core formation.

4. CHEMISTRY OF PRESTELLAR MOLECULAR CORES

4.1. Background

The presence of gas-phase chemical inhomogeneities within molecular clouds has been known for some time. In particular, spatial differences in emission morphologies

between carbon chains (e.g., HC_3N, C_2S) and nitrogen-hydrogen molecules (NH_3, N_2H^+) on scales of 0.05–0.2 pc were described (Suzuki et al. 1992, Pratap et al. 1997). Surveys of numerous cores in Taurus revealed larger emission sizes and velocity linewidths for CS when compared to NH_3, despite similar line centroids (Zhou et al. 1989). These differences have generally been attributed to the slower timescales to activate the nitrogen chemistry, as opposed to the carbon chemistry, or perhaps owing to some dynamical cycling of material that can enhance the carbon chemistry (see van Dishoeck & Blake 1998, Langer et al. 2000, for a discussion of general chemistry).

In this regard two low-mass cores, TMC-1 and L134N, were isolated and studied as template objects because of their rich chemistry and because they are unassociated with star-formation activity (Swade 1989, Hirahara et al. 1992, Pratap et al. 1997). Over 1000 papers have been written for these two objects alone. In general chemical studies computed average line-of-sight abundances using a technique outlined in Irvine et al. (1987). H_2 does not emit appreciably at the cold temperatures associated with these objects (T $\sim$ 10 K). Therefore optically thin isotopologues of CO, generally $C^{18}O$, were used as surrogates to trace the H_2 column density with previously calibrated abundances [e.g., $x(C^{18}O) \sim 1.7 \times 10^{-7} \equiv n(C^{18}O)/n(H_2)$; Frerking et al. 1982]. These studies strongly aided the interpretation that chemical reactions between ions and molecules dominate the gas-phase chemistry (Herbst 2005).

In parallel to gas-phase chemical studies, the fundamental vibrational modes of solid state molecules such as H_2O and CO were detected in the interstellar medium (Gillett & Forrest 1973, Lacy et al. 1984). Many studies of molecular ices frozen on the surfaces of dust grains have been conducted toward embedded sources, which provide a strong IR background to study foreground ices (e.g., van Dishoeck 2004). To provide important insight on ices in cold gas, observations of bright field stars located behind molecular cloud material (with extinctions $\leq$20 mag) are used as candles that probe material remote from embedded sources (Whittet et al. 1988). Icy mantles coating grains in ambient gas are dominated by H_2O ice with substantial amounts of CO and CO_2 at a level of $\sim$25% of the water ice abundance in each case (Gibb et al. 2004).

There exists a threshold extinction below which the ice features are not seen, implying that grains are not mantled at low extinction. This threshold varies for each ice component and is different between various clouds. In Taurus, the water ice threshold is $A_V^{th}(H_2O) = 3.2^m \pm 0.1^m$; a comparable threshold is observed for CO_2 ice but for CO $A_V^{th}(CO) = 6.8^m \pm 1.6^m$ (Whittet et al. 2001, 2007; Bergin et al. 2005). The threshold value presumably is related to the formation mechanisms for ices, and in Taurus the relatively low water ice threshold may imply that the water ice forms at a low density where atomic H is available. These observations further demonstrate that ices constitute a substantial fraction of the available carbon and oxygen (van Dishoeck & Blake 1998). Thus CO (and its isotopologues) is not a reliable tracer of the H_2 column when using previously calibrated abundances. In addition, it is clear that grains can act as a catalyst for chemistry on the surface, producing both simple and complex molecules as part of an interchange between the gas and solid phases (Tielens & Hagen 1982, Herbst et al. 2005).

4.2. Observational Chemistry

4.2.1. Gas-phase freeze-out. As discussed in Section 3 a sample of low-mass starless cores are now known with physical structure well-described as a function of position: N_{H_2} (r), $n_{H_2}(r)$, $T_{dust}(r)$, $T_{gas}(r)$. Sample profiles are given in **Figure 4**. Foremost among these are the two new template objects: L1544 and B68. There are some caveats to the determination of each of these parameters, but the overall structure is well characterized and has led to significant advances in our understanding of the chemistry. In general there are two factors that influence these gains. (*a*) Using the dust millimeter/submillimeter continuum emission as a surrogate for the H_2 distribution allows for an examination of molecular abundance variations directly relative to H_2. This is a fact noted by Mezger et al. (1992) in the high-mass NGC2024 star-forming region. However, the presence of embedded sources can substantially influence the dust emission morphology, potentially leading to different conclusions (Chandler & Carlstrom 1996). Although starless cores do have small thermal gradients (Section 3.2) this particular complication is minimized. (*b*) Molecular emission depends on the H_2 density, gas temperature, and on the abundance. Using sophisticated 1D radiation transfer codes (Monte-Carlo or Accelerated Lambda Iteration; Bernes 1979, Rybicki & Hummer 1991) and the density and temperature structure as inputs, the abundance profile along the line of sight can be constrained for the first time.

Initial studies found the first direct link between chemistry in the gas and interactions with grain surfaces by simply comparing the estimated CO and CCS column densities to the H_2 column estimated from the dust (Kuiper et al. 1996, Willacy et al. 1998, Kramer et al. 1999, Caselli et al. 1999). This is interpreted as evidence from gas-phase data that the CO molecules are freezing onto grain surfaces. A comparative study of CO and dust emission suggests freeze-out dominates when densities exceed $\sim 3 \times 10^4$ cm^{-3} (Bacmann et al. 2002).

Spatial mapping of ices within individual cores supports the interpretation of the gas-phase observations as the abundance of CO ice is found to significantly increase when densities exceed $\sim 10^5$ cm^{-3} (Pontoppidan 2006). Near the core center the abundance is close to the typical gaseous CO abundance of 10^{-4}, indicating that the majority of CO is frozen out. Furthermore, the abundance of water ice is typically 0.5×10^{-4} to 0.9×10^{-4} except at the highest densities where the abundance increases (Pontoppidan et al. 2005). The molecular ices are therefore substantial reservoirs of the available oxygen.

4.2.2. Selective freeze-out. Molecular surveys reveal further differences; **Figure 7** shows a sample of this work with a comparison of the 850 μm dust continuum distribution in the Barnard 68 starless core with molecular emission traced by C^{18}O and N_2H^+. In this core the N_2H^+ emission more closely follows that of the dust than does C^{18}O, which appears as a "semi-ring-like" structure around the dust and N_2H^+ emission maximum (Bergin et al. 2002). Tafalla et al. (2002) surveyed five cores in Taurus (including L1544) illustrating general characteristics of core chemistry: carbon-bearing species, represented by CO and CS deplete from the gas while nitrogen-hydrogen bearing molecules, N_2H^+ and NH_3, trace the core center (see
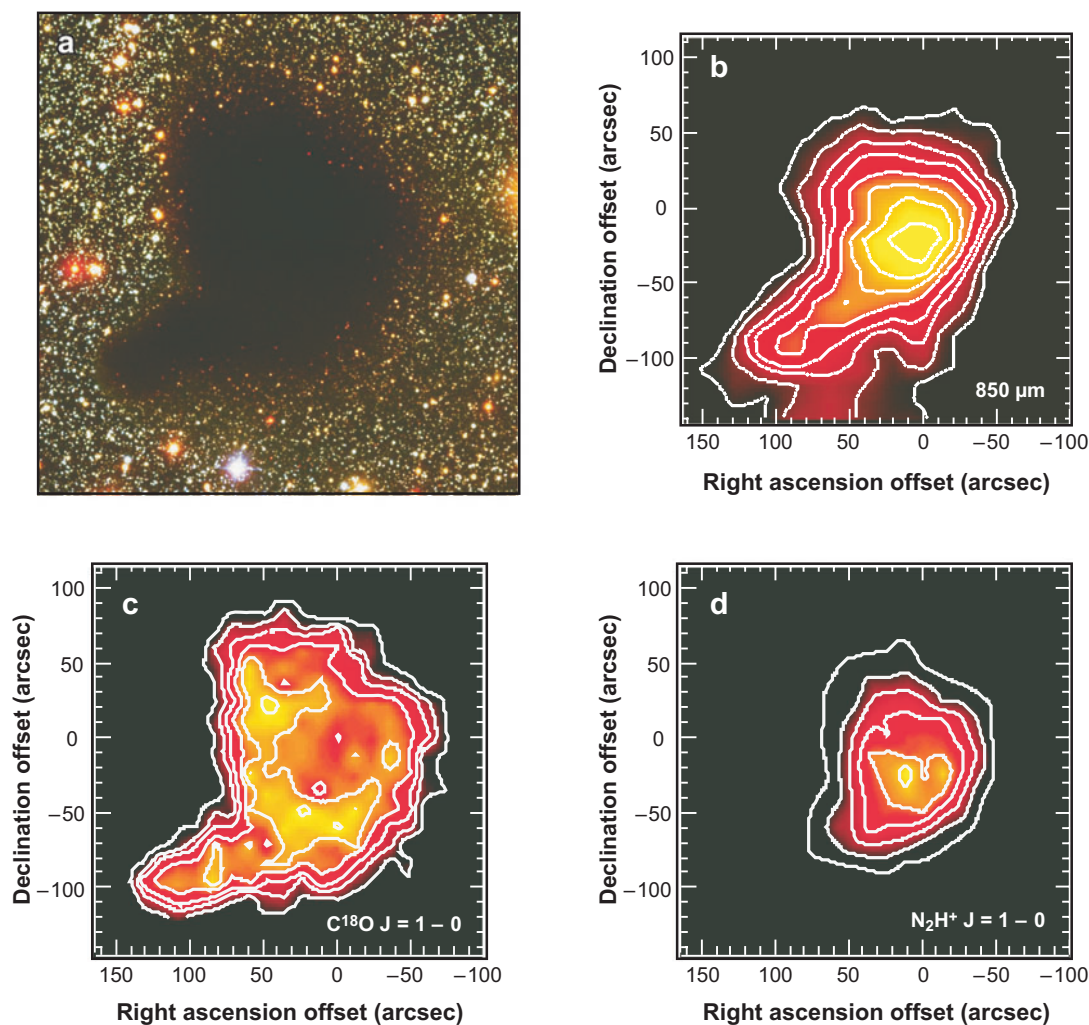
Figure 7

(*a*) A deep optical image of the dark globule Barnard 68 (Alves, Lada & Lada 2001) along with contour maps (*b–d*) of integrated intensity from molecular emission lines of N_2H^+ (contour levels: 0.3–1.8 by 0.3 K km s^{-1}), $C^{18}O$ (0.2–0.7 by 0.1 K km s^{-1}), and 850-μm dust continuum emission (10–70 by 10 mJy beam^{-1}). Molecular data, with an angular resolution of ~25 arcsec, are from Bergin et al. (2002) and dust emission (angular resolution of 14.5 arcsec) from Bianchi et al. (2003).

also Caselli et al. 1999). From the abundance profile it is estimated that the CO and CS abundance traces a large dynamical range with declines of at least 1–2 orders of magnitude in the core centers relative to the lower density core edge, while the abundances of nitrogen molecules either stay constant or decay more slowly. The interpretation of "selective" freeze-out, where molecules exhibit different behavior in

terms of the response of the chemistry to interactions with grain surfaces, naturally explains some long-standing issues such as the emission differences seen between carbon and nitrogen molecules described earlier (compare Swade 1989, Pagani et al. 2005), and the larger core sizes and velocity dispersions seen for CO and CS when compared to earlier NH_3 data (Zhou et al. 1989, Tafalla et al. 2002). For star formation this isolates the nitrogen hydrides as the key probes of dense gas.

4.2.3. Carbon, oxygen, and nitrogen. Cores with well-defined physical properties have clarified additional outstanding chemical issues regarding carbon, oxygen, and nitrogen chemistry. It is clear that CO represents the major reservoir of carbon in the gas and, along with CO_2, in the grain mantle. Maret et al. (2006) demonstrated that N_2 is not the dominant carrier of nitrogen in molecular gas. They suggest NI as a main reservoir of atomic nitrogen (see also van Dishoeck & Blake 1998); however, at present, it is unclear what the predominant form of gas-phase nitrogen is. Observations by the *Submillimeter Wave Astronomy Satellite* (SWAS) and *Odin* also demonstrated that the abundance of ortho-water vapor and molecular oxygen is well below theoretical expectations throughout the Galaxy (Snell et al. 2000, Hjalmarson et al. 2005) and in starless cores in particular (Bergin & Snell 2002). Owing to atmospheric absorption, para-water vapor has yet to be observed and the limits on the water abundance disagree with pure gas-phase chemical theory provided that the ortho/para ratio is not below the equilibrium value at 10 K (o-H_2O/p-H_2O $\sim$ 0.3). The low water vapor abundance is interpreted as the result of water ice formation on grain surfaces. At grain temperatures below $\sim$110 K (Section 4.3.2) water will remain frozen on grains, which indirectly lowers the gas-phase atomic oxygen abundance, thereby hindering formation of water and molecular oxygen in the gas (Bergin et al. 2000, Charnley et al. 2001). Further analysis suggests that the water vapor emission likely arises from the surface photodissociation region where a balance between photodesorption of water ice and photodissociation of water vapor exists (OH should behave in a similar fashion) (Melnick & Bergin 2005). The launch of *Herschel*, which will be capable of observing both ortho- and para-water, will provide definitive information on the water abundance and its potentially defining role in gas-phase freeze-out.

4.3. Chemical Theory

4.3.1. Basic processes. In the literature the loss of gaseous molecules to the solid phase is often labeled as depletion—which implies a lowering of the gas-phase abundance—or as freeze-out, which is a more direct statement of the process. In practice both terms can be used, but there are some nuances. Although neutral species freeze onto grain surfaces it is not thought that molecular ions behave in a similar fashion. Grains in dense clouds are believed to carry negative charge (Weingartner & Draine 2001). The ion–negatively charged grain recombination releases a few eV that, if carried by the products, significantly exceeds the molecule-grain binding energies of $\sim$0.1 − 0.5 eV (Collings & McCoustra 2005). Thus ions can deplete, via, for example, gas-phase processes and by precursor molecules (e.g., CO for HCO^+) adsorbing onto grains, but do not freeze out.

Atoms and molecules freeze onto grain surfaces or adsorb with a rate of $k_{fo} = \sigma v n_g S \, \text{s}^{-1}$. Here σ is the grain cross-section (generally assumed to correspond to an average grain with 0.1 μm radius), v is the mean velocity of the Maxwellian distribution of gaseous particles, n_g is the space density of grains, and S is the sticking coefficient (i.e., how often a species will remain on the grain upon impact). Using relevant parameters for CO at 10 K (assuming $S = 1$ as suggested by laboratory experiments; e.g., Bisschop et al. 2006) the freeze-out timescale $\tau_{fo} = k_{fo}^{-1} \sim 5 \times 10^9 / n_{H_2}$ (cm^{-3}) year. Once on the grain, molecules can react with any species that is mobile on the grain surface at 10 K, such as atomic hydrogen, or if a species is saturated (e.g., H_2O, NH_3, CO_2) it will remain inert on the surface. For cold dense gas that is shielded from external radiation the physical processes that can remove or desorb molecules from grain surface are either inactive or can only desorb the most volatile ices (see van Dishoeck & Blake 1998 for a complete summary of desorption processes). In cold cores it is thought that energetic cosmic ray impacts can desorb the most volatile ices (e.g., CO but not H_2O; Leger et al. 1985, Hasegawa & Herbst 1993, Bringa & Johnson 2004). Thus the dominant effect is the adsorption of atoms and molecules onto grain surfaces and any subsequent consequences that result from this interaction.

4.3.2. Chemical and dynamical timescales. In **Figure 8** we compare relevant chemical and dynamical timescales. Representative dynamical timescales are provided for free-fall and ambipolar diffusion, the latter having been suggested as a primary mode of core condensation (Shu, Adams & Lizano 1987). The free-fall timescale is $\tau_{ff} = [3\pi/32G\rho]^{0.5} \sim 4 \times 10^7 / n_{H_2}^{0.5}$ years and the ambipolar diffusion timescale is
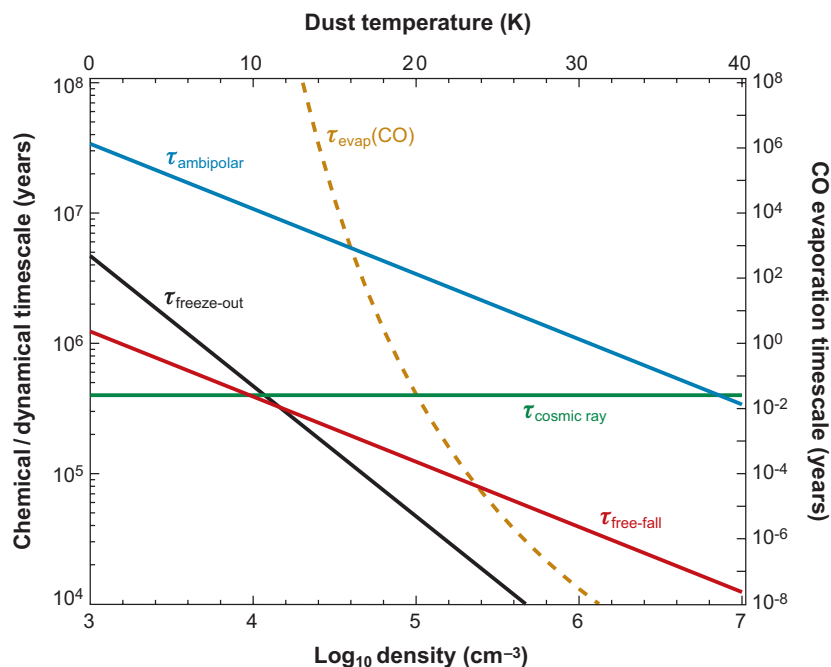

Figure 8

Plot of various chemical and dynamical timescales shown as a function of the molecular hydrogen volume density. Also shown is the density independent CO evaporation timescale as a function of the dust temperature (which, in the plot, is also not a function of the density). Relevant equations for each quantity are provided in Section 4.3.2 and Section 4.4.2. In this plot the cosmic ray timescale is set by the time for any change from an equilibrium state to be reset by cosmic ray powered chemistry. The ambipolar diffusion term assumes $x_e = 2 \times 10^{-8} (n_{H_2}/10^5 \, \text{cm}^{-3})^{-0.5}$.

discussed in Section 4.4.2. The gas-phase chemical timescale is set by cosmic rays and has a constant dependence on the density, while freeze-out has linear dependence on the density. The evaporation rate is given by the Polanyi-Wigner relation (Tielens 2005):

$$\tau_{evap} = \nu_0^{-1} \exp(E_b/kT)(s^{-1}), \qquad (1)$$

where ν_0 is the vibrational frequency of the molecule in the potential well (typically $\sim 10^{12}$ s^{-1}) and E_b is the binding energy. The evaporation timescale has an exponential dependence on the dust temperature, but critically depends on the binding strength to the grain surface or mantle. Measured binding energies for CO-CO are ~ 820 K (Collings et al. 2003) and ~ 5800 K for H$_2$O–H$_2$O (Fraser et al. 2001), implying evaporation temperatures of ~ 15 K for CO and ~ 110 K for H$_2$O at $n_{H_2} = 10^5$ cm^{-3} and assuming a typical 0.1 μm grain abundance of $x_{gr} = 10^{-12}$. **Figure 8** demonstrates a key aspect of starless cores—as cold objects, $T_{dust} \sim T_{gas} \sim 10$ K, and evaporation is unimportant, with timescales $>10^8$ yrs. Furthermore the freeze-out timescale becomes shorter than the free-fall and ambipolar diffusion timescales as the density increases. Thus, as the core physically evolves, the effects of freeze-out on gaseous species are magnified and can be used to constrain the mechanism of core formation.

4.3.3. Chemical/dynamical models. Combined chemical and dynamical models follow the chemical composition as the core contracts. Such models generally adopt parameterized fits or a more direct coupling to simple dynamical models (e.g., Larson 1969, Penston 1969, Shu 1977, Basu & Mouschovias 1994). Notable chemical/dynamical models are Rawlings et al. (1992), Bergin & Langer (1997), Aikawa et al. (2001) and Li et al. (2002). With basic gas-grain microphysics incorporated into time-dependent models (see Tielens 2005) the chemical structure discussed in Section 4.2.2 can be explained and, in some cases, was predicted.

Basic elements of the chemistry are illustrated in **Figure 9**. During collapse or condensation, the central regions of the core increase in density to levels where neutrals rapidly freeze onto grains ($n_{H_2} > 10^5$ cm^{-3}). This contrasts with the lower density less evolved core edges with undepleted abundances. As collapse proceeds these effects become amplified (compare the two times provided for CO in **Figure 9**). Bergin & Langer (1997) first showed that carbon- and sulphur-bearing species (e.g., CO, CS, CCS) suffer the greatest effect from depletion. In contrast the nitrogen hydride pool is the least affected (see also Aikawa et al. 2001). At first this was assumed to be due to a lower binding strength of N$_2$ (the precursor molecule for both N$_2$H$^+$ and NH$_3$) to the grain surface than for CO. This has now been measured to be equivalent to CO (Öberg et al. 2005).

It is now recognized that the observational appearance of selective freeze-out can be separated into first-order chemical effects, the direct freeze-out of neutrals (e.g., CO, CCS, CS, N$_2$), and second-order effects, changes created by the imbalance in the chemistry left primarily by the loss of gaseous CO. CO is a major destroyer of molecular ions and its removal from the gas leads to a change in the relative abundance of major charge carriers (Rawlings et al. 1992). Particularly affected is the H$_3^+$ ion,
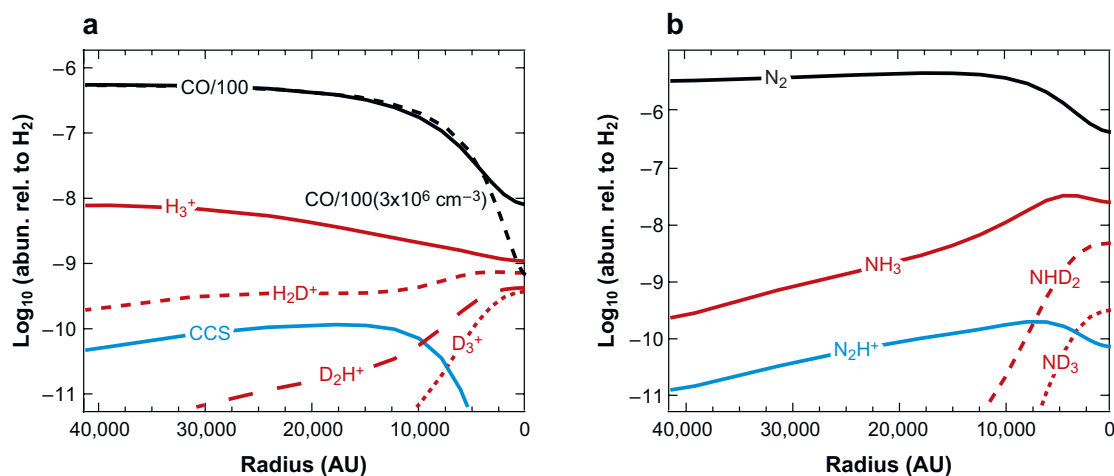
Figure 9

Plot of chemical abundances as a function of core depth for selected species from a chemical
and dynamical model of a contracting Bonnor-Ebert sphere (taken from Aikawa et al. 2005).
All species are shown at a timescale where $n_H(center) = 3 \times 10^5$ cm^{-3}, excluding CO, which
also is shown at $n_H(center) = 3 \times 10^6$ cm^{-3}.

the precursor to molecular ions such as N_2H^+ and HCO^+ that are the respective
daughter products of N_2 and CO. These key observable ions (N_2H^+ and HCO^+)
will also decrease in abundance as the parent molecules freeze out; however, CO is a
major destroyer of N_2H^+, and as CO disappears from the gas there is a subsequent
increase in abundance of N_2H^+ (Aikawa et al. 2001, Bergin et al. 2002, Jørgensen
et al. 2004). NH_3 then forms from N_2H^+ (Geppert et al. 2004, Aikawa et al. 2005).
Thus the abundance of the nitrogen hydrides is strongly enhanced and these species
are probing the gas where CO (and other carbon-bearing species) are depleting. An
important point here is that the abundance of both NH_3 and N_2H^+ are several orders
of magnitude below the abundance of molecular nitrogen. N_2 is freezing onto grains
at the same level as CO. Provided the N_2 abundance does not decrease to levels below
N_2H^+ and ammonia, then these tracers can still form and emit from layers where
commonly observed tracers of dense regions have significantly reduced abundances.

Combined models reproduce not only the pattern of depletions, but also the
column densities observed in L1544 (Aikawa et al. 2001, Li et al. 2002). In general,
models obtain best agreement with collapse timescales much shorter than would
proceed from ambipolar diffusion starting from a magnetically subcritical state (e.g.,
Walmsley et al. 2004); however there is some disagreement (Li et al. 2002). A clear
point is that evolutionary timescales at densities near $\sim 10^4$ cm^{-3} cannot be much
longer than $\sim 0.5 - 1$ Myr as significant CO freeze-out would be produced at densities
below where it is observed (Flower et al. 2005, Tafalla et al. 2006). Moreover, collapse
cannot be too fast (>0.2 km s^{-1} at τ_{dyn} > 5 × 10^5 years). [The typical nonthermal
linewidth in starless cores (e.g., L1498, L1517B, B68, etc.) is 0.2 km s^{-1}. If this
represents a purely inward motion, it would correspond to an infall speed of 0.1 km s^{-1}

at most. With a typical core radius is 0.05 pc, this implies a typical contraction time of 0.5 Myr.] Otherwise there will be less depletion, and emission linewidths would be too broad (Myers 1983).

Current work has greatly benefited from laboratory work on low-temperature gas-phase reactions, grain binding energies, and on surface catalysis (Katz et al. 1999, Hornekær et al. 2003, Collings & McCoustra 2005, Nagaoka et al. 2005, Bisschop et al. 2006, Florescu-Mitchell & Mitchell 2006). Moreover the recent recalculation and extension of collisional rates of astrophysically important molecules is of great use and deserves mention (Flower 2001, Dubernet & Grosjean 2002, Daniel et al. 2005). However, large questions remain regarding the nature of the grain surface catalysis in this cold environment and the strength of the mechanisms that could return molecules to the gas (e.g., Leger et al. 1985, Bringa & Johnson 2004, Shen et al. 2004). It is also unclear how complex molecules form in the gas phase. For example CH_3OH is detected in cold clouds, but currently has no known gas-phase formation route. An examination of the extent of the complex chemistry in cores with well-defined properties is needed and will likely lead to gains in our understanding of interstellar organic chemistry (see Hirota et al. 2004).

One clear positive statement is that our knowledge of the chemistry and the time-sensitive nature of the gas-grain interaction is such that we now have the methods to place relative ages between cores within a given sample (Hirota et al. 2002, Tafalla & Santiago 2004). This should aid in our analysis of the core/star formation process. Moreover, the combination of chemical/dynamical models with radiative transfer (see Lee et al. 2004, as an example) offers the best opportunity to take these models to the next level and truly begin to test star-formation theory.

4.4. Deuterium Chemistry and the Ionization Fraction

4.4.1. Deuterium fractionation. Another second-order effect induced by the CO freeze-out is a sharp rise in the level of deuterium fractionation. Enhancements of deuterium-bearing molecules relative to the hydrogen counterparts have been known for some time (Guelin et al. 1982). In cold clouds enrichments of 2–3 orders of magnitude are observed above the atomic hydrogen value of (D/H) $\geq (2.3 \pm 0.2) \times 10^{-5}$ estimated within 1 kpc of the Sun (Linsky et al. 2006). Because of the lower zero-point energy of deuterium bonds compared to bonds with hydrogen, ion-molecule reactions in the dense interstellar medium are thought to be the mechanism responsible for these enrichments (Millar et al. 1989). Deuterium enrichments can also be created via reactions on the surfaces of dust grains (Tielens 1983, Nagaoka et al. 2005), but in these cold cores freeze-out is believed to dominate as opposed to sublimation (e.g., freeze-out dominates the chemistry of the volatile CO molecule).

In the cold dense interstellar medium, deuterium chemistry is driven by the following reaction:

$$H_3^+ + HD \leftrightarrow H_2D^+ + H_2 + 230\,K. \tag{2}$$
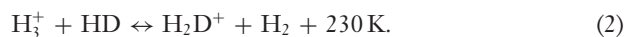
The forward reaction is slightly exothermic favoring the production of H_2D^+ at 10 K, enriching the [D]/[H] ratio in the species that lie at the heart of interstellar

ion-molecule chemistry (Millar et al. 1989). [Reaction 2 has been measured in the lab at low temperatures. The finding is that there is an additional dependence on the ortho/para ratio of H_2 (Gerlich et al. 2002).] These enrichments are then passed down the reaction chains to species such as DCO^+, DCN, HDCO, and others.

Pure gas-phase models without freeze-out cannot produce significant quantities of doubly (NHD_2; Roueff et al. 2000) and triply deuterated ammonia (ND_3; Lis et al. 2002) as observed in starless cores. This motivated a re-examination of the basic deuterium chemistry. The primary advance in our understanding is twofold: (*a*) deuteration reactions do not stop with H_2D^+, rather they continue toward the formation of both D_2H^+ and D_3^+ via a similar reaction sequence (Phillips & Vastel 2003, Roberts et al. 2003, Walmsley et al. 2004):

$$H_2D^+ + HD \leftrightarrow D_2H^+ + H_2 + 180\,K, \tag{3}$$

$$D_2H^+ + HD \leftrightarrow D_3^+ + H_2 + 230\,K. \tag{4}$$
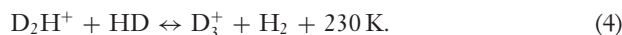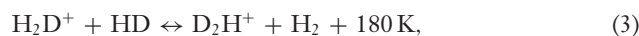
(*b*) The freeze-out of CO, which is the primary destroyer of both H_3^+ and H_2D^+, increases the rate of the gas-phase fractionation reactions (see deuterium species in **Figure 9**; Stark et al. 1999, Aikawa et al. 2001, Bacmann et al. 2003). This inference is strongly supported by the detection of H_2D^+ and D_2H^+ in starless cores (Caselli et al. 2003, Vastel et al. 2004, van der Tak et al. 2005), as illustrated in **Figure 10**.

The creation of multiply deuterated ions leads to the production of high deuteration levels similar to those observed. An additional by-product is an enhanced atomic (D/H) ratio that will accrete onto grains and be available for surface reactions (Tielens 1983, Charnley et al. 1997, Stantcheva & Herbst 2003, Aikawa et al. 2005) creating
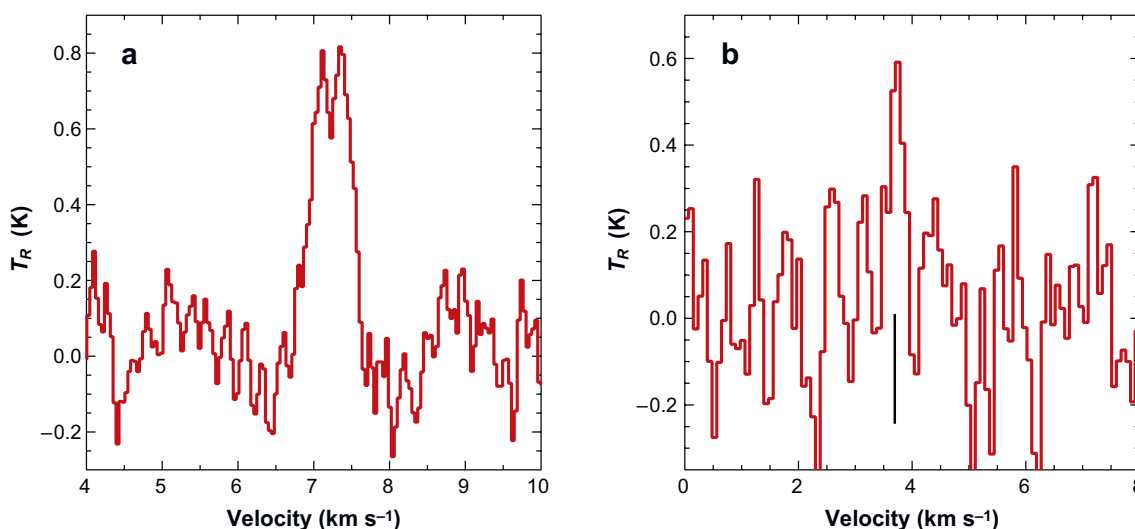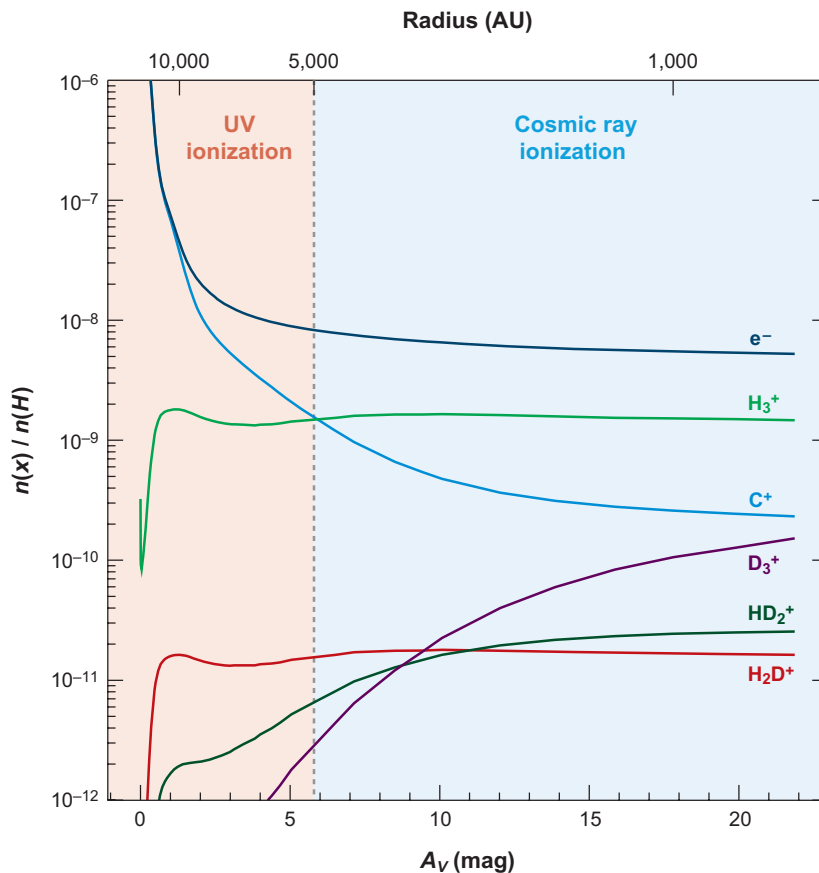

Figure 10

(*a*) Detection of H_2D^+ emission in L1544 (Caselli et al. 2003, van der Tak et al. 2005). (*b*) 4.4σ detection of D_2H^+ in the starless core IRAS16293E (Vastel et al. 2004).

molecules rich in deuterium to be exposed when ices sublimate off warm grains as the result of stellar birth. However, the extent of the surface deuteration opposed to the gas phase needs to be further explored. It is worth emphasizing that the observed form of H_2D^+ in interstellar clouds is ortho-H_2D^+, and models show that the H_2D^+ ortho/para ratio (o/p) will change with density and is a sensitive function of the molecular hydrogen ortho/para ratio (Flower et al. 2006). If the H_2 o/p ratio is not in equilibrium at the low $T_g < 20$ K (where $o/p \ll 1$) and instead is near 3:1, then deuterium fractionation will not work (Pineau des Forêts et al. 1991, Gerlich et al. 2002). Observations from *Spitzer* suggest that the H_2 o/p ratio is in equilibrium in cold preshock gas (Neufeld et al. 2006), a fact consistent with the observed fractionation. *Herschel* and SOFIA will be needed to constrain the H_2 o/p ratio via observations of ortho- and para-H_2D^+ in starless cores.

4.4.2. Ionization fraction. For subcritical starless cores (where the magnetic field supports the cloud against gravity, Section 2.7) the evolutionary timescale is set by ambipolar diffusion and the ion fraction is a critical factor in determining the magnetic flux leakage. McKee (1989) discussed the various charge carriers and recombination rates and derived a basic expression that has wide use: $x_e = 1.3 \times 10^{-5} n(H_2)^{-0.5}$. The effects of freeze-out can alter both the prefactor and the exponent of the density dependence (Bergin & Langer 1997, Caselli et al. 2002c, Walmsley et al. 2004, but see also Ciolek & Mouschovias 1998).

Past studies of the ion fraction in dense cores focused on the DCO^+/HCO^+ ratio, which was predicted to be a sensitive function of the electron abundance. Furthermore, it was thought that HCO^+ was a major charge carrier throughout the core (e.g., Caselli et al. 1998, Williams et al. 1998). These studies found line-of-sight average ion fractions of $x_e \sim 10^{-7}$ (relative to H_2), implying weak coupling to the magnetic field. One variable assumption in models is the presence or absence of metal ions (e.g., Fe^+, Mg^+, ...), which have slower recombination timescales than molecular ions. If present, metals could dominate the electron fraction over molecular ions ultimately produced by cosmic ray impacts. Currently, detailed models imply no significant contribution from heavy metal ions to the electron fraction (Caselli et al. 2002c, Maret et al. 2006).

Owing to the freeze-out of neutrals, HCO^+ does not trace the core center and major charge carriers in the core center are likely to be a combination of H_3^+, H_2D^+, D_2H^+, and D_3^+. An example of the typical ionization structure is given in **Figure 11**. When illuminated by the standard interstellar radiation field or below, the ionization is high at core edges ($A_V < 1$–2 mag) owing to CO photodissociation and ionization of carbon. Deeper in the cloud the regime of cosmic ray ionization leads to an ion fraction that decays with increasing density. For the densest ($n_{H_2} > 10^6$ cm^{-3}), most evolved cores, the ultimate expectation is that D_3^+ is the dominant ion (Roberts et al. 2003, Walmsley et al. 2004). Observations and models now suggest that in at least some objects the ion fraction in the core center is quite low, $x_e \sim 3 \times 10^{-9}$, implying that the gas is locally decoupled from the field (i.e., the timescale for ambipolar diffusion is comparable to or less than the free-fall time, Caselli et al. 2002c, van der Tak et al. 2005).

Figure 11

Derived electron fraction and major ion abundances in the Barnard 68 core. Abundances are relative to H nuclei. Zones where the ionization is dominated by UV and Cosmic Ray are delineated (effectively where C^+ is no longer the most abundant ion). In this plot H_3^+ is the main ion, carrying $\sim 20\%$ of the charge with the remainder contained in more complex ions. (Taken from S. Maret & E.A. Bergin, in preparation) Some uncertainties in these calculations include the gas-grain model (i.e., the assumed binding strengths and desorption mechanisms) and the cosmic ray ionization rate.

Walmsley et al. (2004) and Flower et al. (2005) discussed ambipolar diffusion timescales in the context of depletion, providing detailed expressions:

$$\tau_{ad} \sim \frac{2}{\pi G m_{H_2}^2} \sum_i \frac{n_i}{n_{H_2}} \mu_{in} \langle \sigma v \rangle_{in} \text{ year,} \qquad (5)$$

where G is the gravitational constant, i implies a summation of ionic species, and $\mu_{in} = m_i m_{H_2}/(m_i + m_{H_2})$ is the reduced mass with H_2 the neutral collision partner. The rate coefficient for momentum transfer between ions and neutrals is assumed to be $\langle \sigma v \rangle_{in} = \pi e(\alpha/\mu_{in})^{0.5}$, with α as the polarizability of H_2 (Osterbrock 1961). If HCO^+ is the dominant ion, then $\tau_{ad} \sim 1.7 \times 10^{14} x_e$. An essential feature is that the timescale is proportional to the square root of the reduced mass implying that the ionic composition also influences the diffusion of magnetic flux (the timescale is $\sim 60\%$ lower if H_3^+ dominates and 25% for D_3^+). These researchers highlight the potential of negatively charged grains to alter the degree of ionization and also as limiting factors in deuterium fractionation, which can be influenced by the changing size distribution as the result of coagulation.

4.5. Key Tracers and the Possibility of Complete Heavy Element Depletion

Starless cores have revealed a dynamic and evolving chemical structure that points to key tracers that probe different depths and evolutionary times. One open possibility is that all heavy elements are depleted in core centers prior to stellar birth. This has important implications for our ability to study the process because the heavy element species (e.g., CO, CS, N_2H^+, ...) have permanent dipole moments and can be observed via pure rotational transitions in regions of the atmosphere with good transmission via heterodyne techniques at millimeter wavelengths. If the timescales of star formation are such that heavy element depletion occurs prior to the formation of a point source then our ability to study the entire process will be severely hampered, leaving only hydrogen/deuterium molecules with dipole moments as probes (H_2D^+, D_2H^+).

At present the evidence for total heavy element depletion is inconclusive and focused on the question of whether N_2H^+ is seen to deplete. This molecule is key as it also is the likely formation route of NH_3, and if it depletes then ammonia should follow suit. Bergin et al. (2002) and Maret et al. (2006) find that N_2H^+ does drop in abundance toward the center of the B68 core. In contrast, the N_2H^+ and NH_3 emission in L1544 when observed in high resolution appears to coincide with the continuum emission peak (Williams et al. 1999, Crapsi et al., in preparation). Thus in the two best-studied sources we find contradictory solutions and total heavy elemental depletion remains an intriguing possibility.

Given the gains in our understanding of the chemistry and how it changes with core evolution, in **Figure 12** we provide a schematic to summarize our current knowledge. For less evolved sources ($n_{r=0} < few \times 10^4$ cm^{-3}) the effects of depletion are likely minimized and commonly observed molecules such as CO, C^{18}O, CS, and HCO$^+$, remain viable tracers. For evolved sources ($n_{r=0} > few \times 10^4$ cm^{-3}), species such as N_2H^+, NH_3, N_2D^+, and DCO$^+$ appear to be the best molecular probes of core gas, perhaps even to the dense center. Regardless of whether total heavy element depletion has occurred, both H_2D^+ and D_2H^+ are unambiguous tracers of the densest gas. In contrast, emission from C^{18}O, CS, H_2O, OH, and HCO$^+$ preferentially sample the core edge.

5. INFRARED DARK CLOUDS

5.1. Background

Infrared dark clouds (IRDC) were discovered serendipitously in mid-IR surveys of the Galactic plane by the *Infrared Space Observatory*'s ISOGAL survey (Perault et al. 1996; ISOGAL consisted of a 7- and 15-μm survey of 12° in the plane interior to $|l| = 45°$) and the *Midcourse Space Experiment* (MSX; Egan et al. 1998). (MSX surveyed from $l = 91 - 269°$ with $b \pm 5°$ in five filters sampling between 4–25 μm. IR dark clouds are best seen in MSX Band A images.) Both surveys revealed a population of objects that were dark at mid-IR wavelengths with opacities ranging from 1 to 4 at 8 and 15 μm (Carey et al. 1998, Hennebelle et al. 2001). The objects appear to be quite filamentary and comparison with IRAS suggests that the objects were dark from

Major gas-phase tracers in starless cores
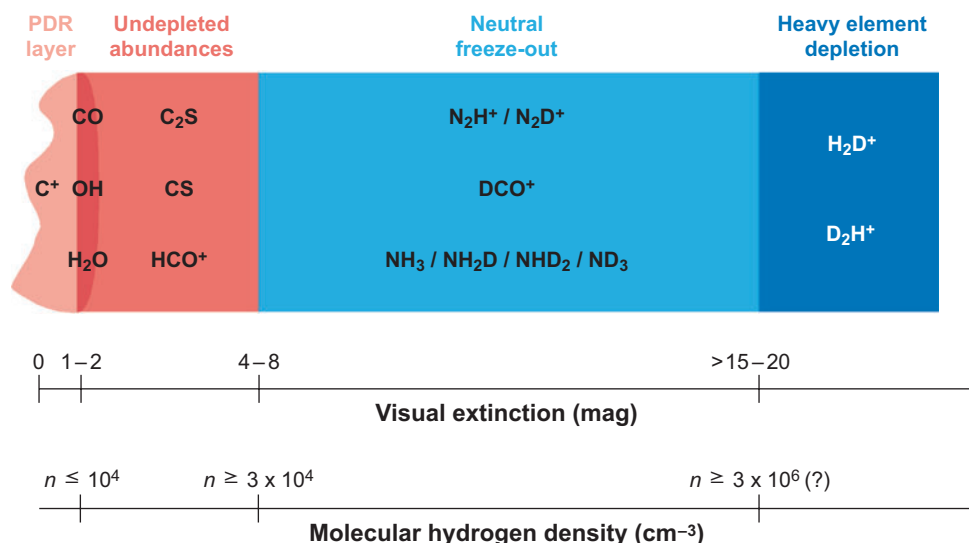
Figure 12

Schematic summary of the major gas-phase probes of starless cores as a function of depth and density. The scales provided are approximate and were estimated from Barnard 68. In this schematic the temperature is assumed to be low (<15 K) below $A_V \sim 2$ mag.

7 to 100 µm and "represent a population of heretofore unrecognized population of cold, dense, isolated clouds" (Egan et al. 1998, Hennebelle et al. 2001). A compilation of MSX dark objects finds over 10,000 sources with kinematic distances between 1–8 pc with a distribution that peaks toward prominent star-forming regions, spiral arm tangents, and the 5-kpc Galactic Molecular Ring (Simon et al. 2006). **Figure 13** presents one example showing the G11.11–0.12 IRDC as seen by *Spitzer* and in submillimeter continuum emission.

Much of the interest generated by this discovery focuses on the formation of high-mass stars and stellar clusters. This review demonstrates many of the gains in our knowledge of the formation of low-mass stars through the isolation of starless cores as a unique sample to study the initial conditions of star formation. In the case of clustered star formation, the nearest region is Orion at ∼500 pc and it is unclear how representative Orion is when compared to star formation in the inner Galaxy, where most of the molecular mass resides. IRDCs provide the capability to examine the early stages of star cluster formation beyond the local solar neighborhood. The primary issue for massive star formation is that the timescales are much faster when opposed to the formation of solar mass stars. Thus there will be fewer prestellar massive objects present at any given time to isolate. Moreover, because massive stars are born in more distant clouds with stellar clusters the chances of confusion are greater (for a nice review, see Garay & Lizano 1999). The discovery of IRDCs provides a
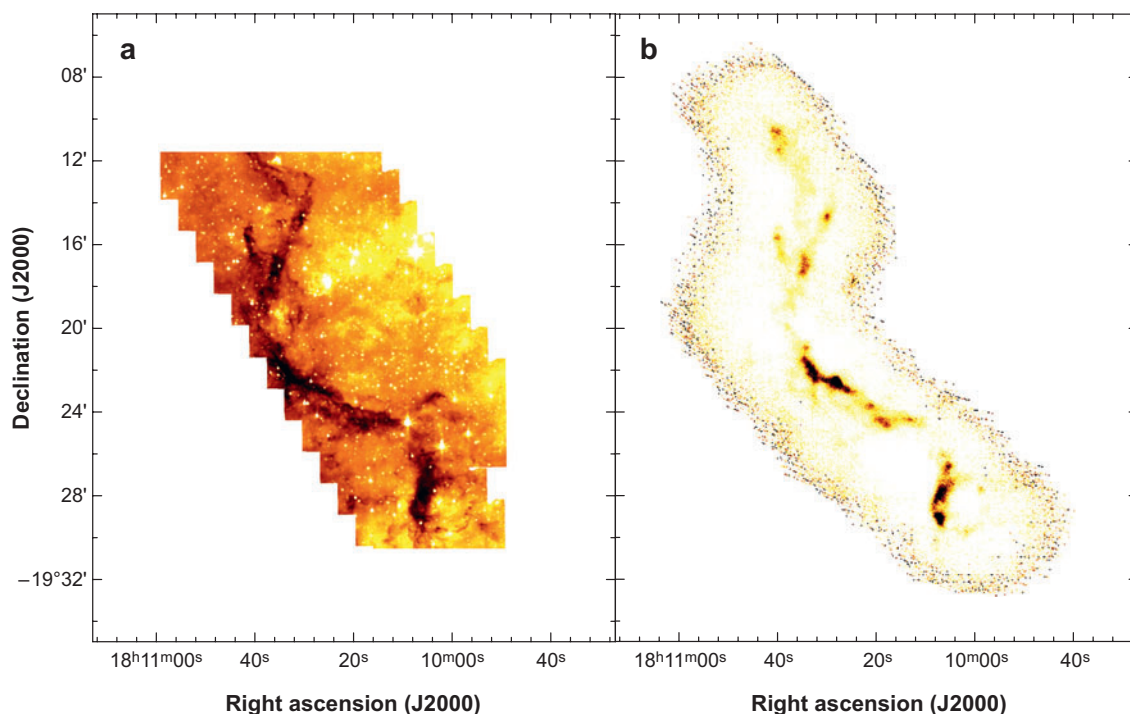
Figure 13

G11.11–0.12 IR dark cloud as seen by (*a*) *Spitzer* IRAC band 4 and (*b*) 850-μm submillimeter
continuum emission (Johnstone et al. 2003). In the *Spitzer* image the bright IR background is
provided by polycyclic aromatic hydrocarbon emission within the 8-μm band and the cloud
appears in absorption. In contrast, the submillimeter continuum emission highlights the dense
regions seen in absorption in the mid-IR.

new—greatly expanded—sample to search for the precursors to massive stars. With-
out constraining observations, theories of massive star formation are divided between
models that suggest that high-mass stars form by accretion of an extended envelope
or competitive accretion of cluster stars for remaining unbound gas, with stars located
near the central potential obtaining higher masses (Krumholz et al. 2005, Bonnell &
Bate 2006). A discussion of the theoretical issues is beyond the scope of this review
and the reader is referred to the cited references and the contribution by Zinnecker
& Yorke in this volume.

5.2. Physical Properties and Implications

The properties of IRDCs have been estimated using a variety of techniques that
have been outlined in Section 3 and Evans (1999). From observations of CO, NH_3,
CH_3C_2H, and H_2CO, temperatures are estimated to be below 20 K with densities
in excess of 10^5 cm^{-3} (Carey et al. 1998, Teyssier et al. 2002, Pillai et al. 2006).
Surveys of millimeter/submillimeter continuum emission and N_2H^+ constrain typical

core masses of 100–1000 $M_\odot$ and sizes of $R \sim 0.3 - 0.7$ pc, which are comparable to those of molecular cores containing embedded high-mass protostellar objects. (Sridharan et al. 2005, Ragan et al. 2006, Rathborne et al. 2006). The cores are dominated by turbulence with velocity linewidths of $\sim 2 - 3$ km s^{-1}. These linewidths are systematically less than seen toward cores with embedded protostars, which is similar to the dependence observed in local clouds (Sridharan et al. 2005, Ragan et al. 2006). The core mass spectrum has a power-law slope of 2.1 ± 0.4 (Rathborne et al. 2006), which is comparable to the Salpeter IMF; however, it is likely that these objects will fragment on scales below the observed resolution (11 arcsec), and this value is also consistent with the CO mass spectrum of molecular clouds (Section 2.3.4). Based on current evidence, it is clear that these sources likely represent the birth sites of stellar clusters and that a subsample must be forming massive stars.

The implications of IRDCs for Galactic star formation have been discussed by Rathborne et al. (2006) who estimate that the star-formation rate in these objects is ~ 2 $M_\odot$/year. This is comparable to the total Galactic rate of 3–5 $M_\odot$/year (Prantzos & Aubert 1995) and hints that this population is responsible for current star formation in the Milky Way. The full promise of these objects will be realized as *Spitzer* Galactic plane surveys (GLIMPSE and MIPSGAL) are analyzed and sensitive high resolution instruments are brought to bear (e.g., CARMA, PdB, eVLA, ALMA) to provide the kind of spatial resolution that is currently available toward the Orion Molecular Cloud. Such observations, when combined with the techniques developed for local starless clouds described in Sections 3 and 4, will ultimately aid in constraining the fragmentation of molecular clouds and the eventual formation of stellar clusters including massive stars.

6. SUMMARY AND FUTURE PROSPECTUS

Cold dark clouds are a fundamental component of the Galactic interstellar medium. They represent the nearest sample of star-forming molecular material, and as such, they play a key role in unraveling the still mysterious process via which stars and planetary systems are born. As this review has shown, the study of dark clouds has seen some significant progress but still contains significant areas of uncertainty.

On the large parsec-scale, high-resolution maps of optical and IR extinction have provided a needed "big picture" look at cloud structure, and have helped to determine that a significant amount of material lies at low extinction ($A_V < 3$–5). Complementing these data are maps of molecular emission where, aided by improved sensitivity and millimeter-wave heterodyne arrays, we can probe deeper using ^{13}CO and C^{18}O than allowed by optically thick ^{12}CO lines. These data have highlighted the filamentary and irregular structure of molecular clouds, suggestive of a transient nature. The velocity structure, on the other hand, tells a tale of the dominance of turbulence, and sophisticated techniques to characterize gas motions have constrained the spectrum of turbulence allowing us to move one step beyond Larson's Laws. Magnetohydrodynamic models have matured to the point where they can produce realistic turbulence, and numerous simulations have shown that the decay of magnetohydrodynamic turbulence is rapid and unavoidable without a continuous source of replenishment. This

raises an important challenge to established theories of long-lived clouds (>10 Myr). In addition to turbulence, static magnetic fields are a potentially important ingredient of cloud physics. Measurements of this field show that in some instances the polarization vectors follow cloud structure, but the measurement and interpretation are complicated by various effects.

In regions where turbulence has dissipated, dense self-gravitating cores form. By mapping their molecular line and dust continuum emission, we have found that cores are characterized by a central region with near-constant density and gas temperature (to within a factor of two), together with subsonic motions. BE spheres often provide accurate fits to the observed emission, and although they represent a simplification of the core physics, they should be considered the best available starting point for numerical models of core evolution. As in the case of the large-scale, the role played by the magnetic field is still uncertain. In addition, detailed radiation transfer analysis suggest the presence of motions along the line of sight. These motions may have an inward component that is associated with core condensation, but often contain additional contributions of an unknown origin. Core-envelope velocity differences, pulsation, or rotation may be responsible for them.

Knowledge of core physical structure has revealed the complex chemical composition of starless cores. Observations demonstrate that chemical inhomogeneities are an inherent dense cold core characteristic that needs to be considered when interpreting molecular line data. The combination of sophisticated radiation transfer codes and realistic core physical structures allows, for the first time, the investigation of line-of-sight chemical gradients. As a result, it has been found that gas-grain interactions dominate the chemistry of cores, and this has a number of consequences. The primary effect is the freeze-out onto grains of important gaseous species, such as CO. This removal of CO from the gas phase leads to the production of new species, like N_2H^+ and NH_3, in the denser gas where these effects are dominant. In addition, the deuterium fractionation of the core is greatly enhanced, as multiply deuterated molecules are produced via reactions that begin with H_2D^+, D_2H^+, and D_3^+. Thanks to this new understanding of the core chemistry, the observed abundance profiles are beginning to be successfully reproduced by models that combine chemistry and dynamics of core contraction. Using these models we can now isolate molecular probes that target specific regions along the line of sight. For example, two classical probes of core structure, CO and CS, are now understood to be only tracers of the low-density cloud surface. Deeper layers of the core are traced by N_2H^+ and NH_3 (along with their deuterated daughter products), while the center is unambiguously traced by H_2D^+ and D_2H^+. These chemical signatures change as a function of core evolution and may help to trace the history of gas contraction.

FUTURE ISSUES

Within this review we have highlighted areas where progress is needed, and here we discuss some areas where breakthroughs could occur using future instruments and advanced techniques. For the most part we are concentrating on issues that can be addressed via observations.

1. There is considerable need to connect the molecular cloud component with the atomic diffuse interstellar medium. This may illuminate the question of cloud formation, cloud destruction, and the origin of the turbulence in molecular clouds. It will require the combination of mapping observations of HI, extinction, [CII], and CO emission.

2. To address the issue of cloud fragmentation and the potential breakdown in hierarchical structure, it is required that clouds are mapped with a uniform tracer from the large to the small scales. The most likely tracer for this work would be the dust continuum emission, if observations retain sensitivity to large-scale structure, and SCUBA-2 offers the best opportunity in this regard. Molecular tracers will provide needed velocity information. Unfortunately, a wide variety of disparate techniques is currently used to analyze the rich information contained in 3D data cubes. A common description of cloud structure is clearly needed both to intercompare observations of different clouds and to test numerical simulations.

3. The transition from turbulent cloud to the quiescent core regime is a critical element in the evolution toward star formation. In this transition, turbulence dissipates and the cores acquire the flattened density profiles reminiscent of Bonnor-Ebert spheres. Whether the observed subsonic motions represent a key part of this transition should be explored. For this, an improved understanding of the chemistry should help in the selection of a number of molecular tracers to probe different layers. To track turbulent dissipation, a number of cores spanning a range of evolutionary states needs to be isolated and characterized. Millimeter observations with existing and future radio telescopes, preferably with large format heterodyne receiver arrays (e.g., SEQUOIA on LMT), offer the potential to examine these issues.

4. A clear advantage results from the ability to combine measurements of the dust column spanning a range of wavelengths from near-IR absorption to submillimeter emission to examine the dust properties, in particular the mass opacity coefficient. In parallel to understanding how the gas changes with contraction there is an open question as to how dust properties change as the mantles grow and grains coagulate. *Herschel* and SOFIA observations should aid to disentangle the coupled effects of dust temperature and emissivity on dust emission/absorption.

5. Models and observations have mapped a chemical sequence that can track the relative evolutionary status of condensing cores. Observations can be used to provide a rough indication of the evolutionary state, but improved theoretical models are still needed to provide core studies with an accurate chemical clock to test core condensation theories. Further testing of models against observables (e.g., integrated emission and line width) also requires accurate collisional rates, molecular rest frequencies, measurements of

low-temperature gas-phase reaction rates, and studies of the gas-grain interaction in the laboratory.

6. It is not yet clear whether the centers of cores are completely depleted in key elements (C, O, and N) preceding the onset of gravitational collapse, and this has important implications in the ongoing search for star-forming infall. *Herschel*, SOFIA, and especially ALMA will be important instruments to clarify this issue.

7. The emerging field of IR dark clouds holds the promise of unlocking the secrets of massive star formation, which is an area with considerable theoretical controversy. At present it is not certain how IR dark clouds fit into our picture of giant molecular clouds. Are these sources the dense centers of clouds in the Galactic molecular ring, and if so, how do they compare in properties (mass spectrum, size, clumping/fragmentation, turbulence) to the local population of massive star-forming regions exemplified by Orion? Systematic studies with high resolution (<4 arcsec) are needed to bring the study of these objects to the level of detail that currently exists for local clouds. eVLA and ALMA will be important in this regard.

ACKNOWLEDGMENTS

LITERATURE CITED

Aikawa Y, Herbst E, Roberts H, Caselli P. 2005. *Ap. J.* 620:330
Aikawa Y, Ohashi N, Inutsuka SI, Herbst E, Takakuwa S. 2001. *Ap. J.* 552:639
Allen L, Megeath T, Gutermuth R, Myers PC, Wolk S, et al. 2007. See Reipurth et al. 2007, p. 361
Alves JF, Lada CJ, Lada EA. 1999. *Ap. J.* 515:265
Alves JF, Lada CJ, Lada EA. 2001. *Nature* 409:159
André P, Bouwman J, Belloche A, Hennebelle P. 2003. See Curry & Fich 2003, p. 127

André P, Ward-Thompson D, Motte F. 1996. *Astron. Astrophys.* 314:625

Arce HG, Goodman AA, Bastien P, Manset N, Sumner M. 1998. *Ap. J. Lett.* 499:L93

Arons J, Max CE. 1975. *Ap. J. Lett.* 196:L77

Arquilla R, Goldsmith PF. 1986. *Ap. J.* 303:356

Bacmann A, André P, Puget JL, Abergel A, Bontemps S, Ward-Thompson D. 2000. *Astron. Astrophys.* 361:555

Bacmann A, Lefloch B, Ceccarelli C, Castets A, Steinacker J, Loinard L. 2002. *Astron. Astrophys.* 389:L6

Bacmann A, Lefloch B, Ceccarelli C, Steinacker J, Castets A, Loinard L. 2003. *Ap. J. Lett.* 585:L55

Ballesteros-Paredes J, Klessen RS, Mac Low MM, Vázquez-Semadeni E. 2007. See Reipurth et al. 2007, p. 63

Ballesteros-Paredes J, Klessen RS, Vázquez-Semadeni E. 2003. *Ap. J.* 592:188

Ballesteros-Paredes J, Vázquez-Semadeni E, Scalo J. 1999. *Ap. J.* 515:286

Bally J, Stark AA, Wilson RW, Langer WD. 1987. *Ap. J. Lett.* 312:L45

Barnard EE. 1907. *Ap. J.* 25:218

Barnard EE. 1919. *Ap. J.* 49:1–24

Barnard EE. 1927. *Catalogue of 349 Dark Objects in the Sky.* Chicago: Univ. Chicago Press

Basu S. 2000. *Ap. J. Lett.* 540:L103

Basu S, Mouschovias TC. 1994. *Ap. J.* 432:720

Bazell D, Desert FX. 1988. *Ap. J.* 333:353

Beech M. 1987. *Astrophys. Space Sci.* 133:193

Beech M. 1992. *Astrophys. Space Sci.* 192:103

Beichman CA, Myers PC, Emerson JP, Harris S, Mathieu R, et al. 1986. *Ap. J.* 307:337

Benson PJ, Myers PC. 1989. *Ap. J. Suppl.* 71:89

Bergin EA, Alves J, Huard T, Lada CJ. 2002. *Ap. J. Lett.* 570:L101

Bergin EA, Hartmann LW, Raymond JC, Ballesteros-Paredes J. 2004. *Ap. J.* 612:921

Bergin EA, Langer WD. 1997. *Ap. J.* 486:316

Bergin EA, Maret S, van der Tak FFS, Alves J, Carmody SM, Lada CJ. 2006. *Ap. J.* 645:369

Bergin EA, Melnick GJ, Gerakines PA, Neufeld DA, Whittet DCB. 2005. *Ap. J. Lett.* 627:L33

Bergin EA, Melnick GJ, Stauffer JR, Ashby MLN, Chin G, et al. 2000. *Ap. J. Lett.* 539:L129

Bergin EA, Snell RL. 2002. *Ap. J. Lett.* 581:L105

Bernes C. 1979. *Astron. Astrophys.* 73:67

Bianchi S, Goncalves J, Albrecht M, Caselli P, Chini R, et al. 2003. *Astron. Astrophys.* 399:L43

Bisschop SE, Fraser HJ, Öberg KI, van Dishoeck EF, Schlemmer S. 2006. *Astron. Astrophys.* 449:1297

Blitz L. 1993. See Levy & Lunine 1993, p. 125

Blitz L, Shu FH. 1980. *Ap. J.* 238:148

Blitz L, Williams JP. 1997. *Ap. J. Lett.* 488:L145

Bodenheimer P. 1995. *Annu. Rev. Astron. Astrophys.* 33:199

Bohlin RC, Savage BD, Drake JF. 1978. *Ap. J.* 224:132

Bok BJ. 1948. *Centennial Symp.*, *Harvard Obs. Monogr. No. 7*, p. 53

Bok BJ. 1977. *Publ. Astron. Soc. Pac.* 89:597

Bok BJ, Reilly EF. 1947. *Ap. J.* 105:255

Bonnell IA, Bate MR. 2006. *MNRAS* 370:488

Bonnor WB. 1956. *MNRAS* 116:351

Bourke TL, Myers PC, Robinson G, Hyland AR. 2001. *Ap. J.* 554:916

Bringa EM, Johnson RE. 2004. *Ap. J.* 603:159

Brunt CM, Heyer MH. 2002. *Ap. J.* 566:289

Brunt CM, Mac Low MM. 2004. *Ap. J.* 604:196

Burke JR, Hollenbach DJ. 1983. *Ap. J.* 265:223

Burkert A, Hartmann L. 2004. *Ap. J.* 616:288

Cambrésy L. 1999. *Astron. Astrophys.* 345:965

Cambrésy L, Beichman CA, Jarrett TH, Cutri RM. 2002. *Astron. J.* 123:2559

Carey SJ, Clark FO, Egan MP, Price SD, Shipman RF, Kuchar TA. 1998. *Ap. J.* 508:721

Caselli P, Benson PJ, Myers PC, Tafalla M. 2002a. *Ap. J.* 572:238

Caselli P, van der Tak FFS, Ceccarelli C, Bacmann A. 2003. *Astron. Astrophys.* 403:L37

Caselli P, Walmsley CM, Tafalla M, Dore L, Myers PC. 1999. *Ap. J. Lett.* 523:L165

Caselli P, Walmsley CM, Terzieva R, Herbst E. 1998. *Ap. J.* 499:234

Caselli P, Walmsley CM, Zucconi A, Tafalla M, Dore L, Myers PC. 2002b. *Ap. J.* 565:331

Caselli P, Walmsley CM, Zucconi A, Tafalla M, Dore L, Myers PC. 2002c. *Ap. J.* 565:344

Ceccarelli C, Caselli P, Herbst E, Tielens AGGM, Caux E. 2007. See Reipurth et al. 2007, p. 47

Chandler CJ, Carlstrom JE. 1996. *Ap. J.* 466:338

Chandrasekhar S, Fermi E. 1953. *Ap. J.* 118:113

Charnley SB, Rodgers SD, Ehrenfreund P. 2001. *Astron. Astrophys.* 378:1024

Charnley SB, Tielens AGGM, Rodgers SD. 1997. *Ap. J. Lett.* 482:L203

Ciolek GE, Basu S. 2000. *Ap. J.* 529:925

Ciolek GE, Mouschovias TC. 1998. *Ap. J.* 504:280

Clemens DP, Barvainis R. 1988. *Ap. J. Suppl.* 68:257

Collings MP, McCoustra MRS. 2005. See Lis et al. 2005, p. 405

Collings MP, Dever JW, Fraser HJ, McCoustra MRS. 2003. *Astrophys. Space Sci.* 285:633

Crutcher RM. 1999. *Ap. J.* 520:706

Crutcher RM, Nutter DJ, Ward-Thompson D, Kirk JM. 2004. *Ap. J.* 600:279

Crutcher RM, Troland TH. 2000. *Ap. J. Lett.* 537:L139

Crutcher RM, Troland TH, Goodman AA, Heiles C, Kazes I, Myers PC. 1993. *Ap. J.* 407:175

Curry CL, Fich M, eds. 2003. *Chemistry as a Diagnostic of Star Formation.* Ottawa: NRC Press

Dame TM, Hartmann D, Thaddeus P. 2001. *Ap. J.* 547:792

Daniel F, Dubernet ML, Meuwly M, Cernicharo J, Pagani L. 2005. *MNRAS* 363:1083

Davis LJ, Greenstein JL. 1951. *Ap. J.* 114:206

del Burgo C, Laureijs RJ. 2005. *MNRAS* 360:901

Di Francesco J, Evans NJ II, Caselli P, Myers PC, Shirley Y, et al. 2007. See Reipurth et al. 2007, p. 17

Dobashi K, Uehara H, Kandori R, Sakurai T, Kaiden M, et al. 2005. *Publ. Astron. Soc. Jpn.* 57:1

Dubernet ML, Grosjean A. 2002. *Astron. Astrophys.* 390:793

Ebert R. 1955. *Zeitschr. Astrophys.* 37:217

Egan MP, Shipman RF, Price SD, Carey SJ, Clark FO, Cohen M. 1998. *Ap. J. Lett.* 494:L199

Ehrenfreund P, Charnley SB. 2000. *Annu. Rev. Astron. Astrophys.* 38:427

Elmegreen BG. 2000. *Ap. J.* 530:277

Elmegreen BG. 2002. *Ap. J.* 564:773

Elmegreen BG, Falgarone E. 1996. *Ap. J.* 471:816

Elmegreen BG, Scalo J. 2004. *Annu. Rev. Astron. Astrophys.* 42:211

Enoch ML, Young KE, Glenn J, Evans NJ II, Golwala S, et al. 2006. *Ap. J.* 638:293

Evans NJ II. 1999. *Annu. Rev. Astron. Astrophys.* 37:311

Evans NJ II, Allen LE, Blake GA, Boogert ACA, Bourke T, et al. 2003. *Publ. Astron. Soc. Pac.* 115:965

Evans NJ II, Rawlings JMC, Shirley YL, Mundy LG. 2001. *Ap. J.* 557:193

Falgarone E, Panis JF, Heithausen A, Perault M, Stutzki J, et al. 1998. *Astron. Astrophys.* 331:669

Falgarone E, Phillips TG, Walker CK. 1991. *Ap. J.* 378:186

Florescu-Mitchell AI, Mitchell JBA. 2006. *Phys. Rep.* 430:277

Flower DR. 2001. *J. Phys. B* 34:2731

Flower DR, Pineau des Forêts G, Walmsley CM. 2005. *Astron. Astrophys.* 436:933

Flower DR, Pineau des Forêts G, Walmsley CM. 2006. *Astron. Astrophys.* 449:621

Fraser HJ, Collings MP, McCoustra MRS, Williams DA. 2001. *MNRAS* 327:1165

Frerking MA, Langer WD, Wilson RW. 1982. *Ap. J.* 262:590

Galli D, Walmsley M, Gonçalves J. 2002. *Astron. Astrophys.* 394:275

Gammie CF, Ostriker EC. 1996. *Ap. J.* 466:814

Garay G, Lizano S. 1999. *Publ. Astron. Soc. Pac.* 111:1049

Geppert WD, Thomas R, Semaniak J, Ehlerding A, Millar TJ, et al. 2004. *Ap. J.* 609:459

Gerlich D, Herbst E, Roueff E. 2002. *Plan. Space Sci.* 50:1275

Gibb EL, Whittet DCB, Boogert ACA, Tielens AGGM. 2004. *Ap. J. Suppl.* 151:35

Gillett FC, Forrest WJ. 1973. *Ap. J.* 179:483

Goldsmith PF. 1987. In *Interstellar Processes*, ed. DJ Hollenbach, HA Thronson, p. 51. Dordrecht: Reidel

Goldsmith PF. 2001. *Ap. J.* 557:736

Goldsmith PF, Langer WD. 1978. *Ap. J.* 222:881

Goldsmith PF, Li D. 2005. *Ap. J.* 622:938

Goldsmith PF, Tang Y, Heyer M, Narayanan G, Snell R, et al. 2005. *Bull. Am. Astron. Soc.* 37:1305

Gonçalves J, Galli D, Walmsley M. 2004. *Astron. Astrophys.* 415:617

Goodman AA, Barranco JA, Wilner DJ, Heyer MH. 1998. *Ap. J.* 504:223

Goodman AA, Bastien P, Menard F, Myers PC. 1990. *Ap. J.* 359:363

Goodman AA, Benson PJ, Fuller GA, Myers PC. 1993. *Ap. J.* 406:528

Goodman AA, Jones TJ, Lada EA, Myers PC. 1995. *Ap. J.* 448:748

Gregersen EM, Evans NJ II. 2000. *Ap. J.* 538:260

Guelin M, Langer WD, Wilson RW. 1982. *Astron. Astrophys.* 107:107

Hartmann L. 2002. *Ap. J.* 578:914

Hartmann L. 2003. *Ap. J.* 585:398

Hartmann L, Ballesteros-Paredes J, Bergin EA. 2001. *Ap. J.* 562:852

Hasegawa TI, Herbst E. 1993. *MNRAS* 261:83

Heiles C, Crutcher R. 2005. In *Cosmic Magnetic Fields*, ed. R Wielebinski, R Beck,
    p. 137. Berlin: Springer-Verlag

Heiles C, Goodman AA, McKee CF, Zweibel EG. 1993. See Levy & Lunine 1993,
    p. 279

Heiles C, Katz G. 1976. *Astron. J.* 81:37

Hennebelle P, Pérault M, Teyssier D, Ganesh S. 2001. *Astron. Astrophys.* 365:598

Henning T, Wolf S, Launhardt R, Waters R. 2001. *Ap. J.* 561:871

Herbst E. 2005. *J. Phys. Conf. Ser.* 4:17

Herbst E, Chang Q, Cuppen HM. 2005. *J. Phys. Conf. Ser.* 6:18

Herschel W. 1785. *Philos. Trans. Ser. I* 75:213

Heyer MH, Brunt CM. 2004. *Ap. J.* 615:L45

Heyer MH, Brunt C, Snell RL, Howe JE, Schloerb FP, et al. 1998. *Ap. J. Suppl.*
    115:241

Heyer MH, Schloerb FP. 1997. *Ap. J.* 475:173

Heyer MH, Vrba FJ, Snell RL, Schloerb FP, Strom SE, et al. 1987. *Ap. J.* 321:855

Hirahara Y, Suzuki H, Yamamoto S, Kawaguchi K, Kaifu N, et al. 1992. *Ap. J.* 394:539

Hirota T, Ito T, Yamamoto S. 2002. *Ap. J.* 565:359

Hirota T, Maezawa H, Yamamoto S. 2004. *Ap. J.* 617:399

Hjalmarson Å, Bergman P, Biver N, Floren HG, Frisk U, et al. 2005. *Adv. Space Res.*
    36:1031

Hornekær L, Baurichter A, Baouche S, Field D, Luntz AC. 2003. *Science* 302:1943

Houde M, Dowell CD, Hildebrand RH, Dotson JL, Vaillancourt JE, et al. 2004. *Ap.
    J.* 604:717

Houghton HE. 1942. *Mon. Not. Astron. Soc. South. Afr.* 1:107

Irvine WM, Goldsmith PF, Hjalmarson Å. 1987. In *Interstellar Processes*, ed. DJ
    Hollenbach, HA Thronson, ASSL, Vol. 134, p. 561. Dordrecht: Reidel

Jackson JM, Rathborne JM, Shah RY, Simon R, Bania TM, et al. 2006. *Ap. J. Suppl.*
    163:145

Jappsen AK, Klessen RS. 2004. *Astron. Astrophys.* 423:1

Jijina J, Myers PC, Adams FC. 1999. *Ap. J. Suppl.* 125:161

Johnstone D, Bally J. 1999. *Ap. J. Lett.* 510:L49

Johnstone D, Di Francesco J, Kirk H. 2004. *Ap. J. Lett.* 611:L45

Johnstone D, Fich M, Mitchell GF, Moriarty-Schieven G. 2001. *Ap. J.* 559:307

Johnstone D, Fiege JD, Redman RO, Feldman PA, Carey SJ. 2003. *Ap. J. Lett.*
    588:L37

Johnstone D, Wilson CD, Moriarty-Schieven G, Joncas G, Smith G, et al. 2000. *Ap. J.* 545:327

Jones CE, Basu S, Dubinski J. 2001. *Ap. J.* 551:387

Jørgensen JK, Schöier FL, van Dishoeck EF. 2004. *Astron. Astrophys.* 416:603

Kandori R, Nakajima Y, Tamura M, Tatematsu K, Aikawa Y, et al. 2005. *Astron. J.* 130:2166

Katz N, Furman I, Biham O, Pirronello V, Vidali G. 1999. *Ap. J.* 522:305

Keto E, Broderick A, Lada CJ, Narayan R. 2006. *Ap. J.* 652:1366

Kirk JM, Ward-Thompson D, André P. 2005. *MNRAS* 360:1506

Kirk JM, Ward-Thompson D, Crutcher RM. 2006. *MNRAS* 369:1445

Klessen RS, Ballesteros-Paredes J. 2004. *Baltic Astron.* 13:365

Koyama H, Inutsuka SI. 2000. *Ap. J.* 532:980

Kramer C, Alves J, Lada CJ, Lada EA, Sievers A, et al. 1999. *Astron. Astrophys.* 342:257

Kramer C, Richer J, Mookerjea B, Alves J, Lada C. 2003. *Astron. Astrophys.* 399:1073

Kramer C, Stutzki J, Rohrig R, Corneliussen U. 1998. *Astron. Astrophys.* 329:249

Krumholz MR, McKee CF, Klein RI. 2005. *Nature* 438:332

Kuiper TBH, Langer WD, Velusamy T. 1996. *Ap. J.* 468:761

Lacy JH, Baas F, Allamandola LJ, Van de Bult CEPM, Persson SE, et al. 1984. *Ap. J.* 276:533

Lada CJ, Alves J, Lada EA. 1999. *Ap. J.* 512:250

Lada CJ, Alves JF, Lombardi M. 2007. See Reipurth et al. 2007, p. 3

Lada CJ, Bergin EA, Alves JF, Huard TL. 2003. *Ap. J.* 586:286

Lada CJ, Kylafis ND, eds. 1999. In *The Origin of Stars and Planetary Systems.* Dordrecht: Kluwer

Lada CJ, Lada EA, Clemens DP, Bally J. 1994. *Ap. J.* 429:694

Lada EA, Strom KM, Myers PC. 1993. See Levy & Lunine 1993, p. 245

Langer WD, van Dishoeck EF, Bergin EA, Blake GA, Tielens AGGM, et al. 2000. See Mannings et al. 2000, p. 29

Larson RB. 1969. *MNRAS* 145:271

Larson RB. 1981. *MNRAS* 194:809

Larson RB. 1995. *MNRAS* 272:213

Larson RB. 2002. *MNRAS* 332:155

Larson RB. 2003. *Rep. Prog. Phys.* 66:1651

Lazarian A, Goodman AA, Myers PC. 1997. *Ap. J.* 490:273

Lazarian A, Pogosyan D. 2000. *Ap. J.* 537:720

Lee CW, Myers PC, Tafalla M. 1999. *Ap. J.* 526:788

Lee CW, Myers PC, Tafalla M. 2001. *Ap. J. Suppl.* 136:703

Lee JE, Bergin EA, Evans NJ II. 2004. *Ap. J.* 617:360

Leger A, Jura M, Omont A. 1985. *Astron. Astrophys.* 144:147

Lehtinen K, Mattila K, Lemke D, Juvela M, Prusti T, Laureijs R. 2003. *Astron. Astrophys.* 398:571

Leung CM, Brown RL. 1977. *Ap. J. Lett.* 214:L73

Levin SM, Langer WD, Velusamy T, Kuiper TBH, Crutcher RM. 2001. *Ap. J.* 555:850

Levy EH, Lunine JI, eds. 1993. *Protostars and Planets III.* Tucson: Univ. Ariz. Press

Li ZY, Shematovich VI, Wiebe DS, Shustov BM. 2002. *Ap. J.* 569:792

Linsky JL, Draine BT, Moos HW, Jenkins EB, Wood BE, et al. 2006. *Ap. J.* 647:1106

Lis DC, Blake GA, Herbst E, eds. 2005. *Astrochemistry: Recent Successes and Current Challenges*, *IAU Symp.*, Vol. 231. Cambridge, United Kingdom: Cambridge Univ. Press

Lis DC, Roueff E, Gerin M, Phillips TG, Coudert LH, et al. 2002. *Ap. J. Lett.* 571:L55

Lizano S, Shu FH. 1989. *Ap. J.* 342:834

Lombardi M, Alves J. 2001. *Astron. Astrophys.* 377:1023

Lombardi M, Alves J, Lada CJ. 2006. *Astron. Astrophys.* 454:781

Loren RB. 1989. *Ap. J.* 338:925

Lovejoy S. 1982. *Science* 216:185

Mac Low MM, Klessen RS. 2004. *Rev. Mod. Phys.* 76:125

Mac Low MM, Klessen RS, Burkert A, Smith MD. 1998. *Phys. Rev. Lett.* 80:2754

Mandelbrot BB. 1983. *The Fractal Geometry of Nature*. New York: Springer

Mannings V, Boss AP, Russell SS, eds. 2000. *Protostars and Planets IV.* Tucson: Univ. Ariz. Press

Maret S, Bergin EA, Lada CJ. 2006. *Nature* 442:425

Mathis JS, Mezger PG, Panagia N. 1983. *Astron. Astrophys.* 128:212

Matthews BC, Wilson CD. 2000. *Ap. J.* 531:868

Matthews BC, Wilson CD, Fiege JD. 2001. *Ap. J.* 562:400

McKee CF. 1989. *Ap. J.* 345:782

McKee CF. 1999. See Lada & Kylafis 1999, p. 29

McKee CF, Zweibel EG, Goodman AA, Heiles C. 1993. See Levy & Lunine 1993, p. 327

McLaughlin DE, Pudritz RE. 1996. *Ap. J.* 469:194

Melnick GJ, Bergin EA. 2005. *Adv. Space Res.* 36:1027

Mestel L, Spitzer L Jr. 1956. *MNRAS* 116:503

Mezger PG, Sievers AW, Haslam CGT, Kreysa E, Lemke R, et al. 1992. *Astron. Astrophys.* 256:631

Miesch MS, Scalo J, Bally J. 1999. *Ap. J.* 524:895

Millar TJ, Bennett A, Herbst E. 1989. *Ap. J.* 340:906

Miller GE, Scalo JM. 1979. *Ap. J. Suppl.* 41:513

Monet D. 1996. *Bull. Am. Astron. Soc.* 28:905

Moneti A, Pipher JL, Helfer HL, McMillan RS, Perry ML. 1984. *Ap. J.* 282:508

Motte F, André P, Neri R. 1998. *Astron. Astrophys.* 336:150

Mouschovias TC. 1976. *Ap. J.* 207:141

Mouschovias TC, Ciolek GE. 1999. See Lada & Kylafis 1999, p. 305

Mouschovias TC, Paleologou EV. 1979. *Ap. J.* 230:204

Mouschovias TC, Tassis K, Kunz MW. 2006. *Ap. J.* 646:1043

Myers PC. 1983. *Ap. J.* 270:105

Myers PC. 1995. In *Molecular Clouds and Star Formation*, ed. C Yuan, J You, p. 47. Singapore: World Sci.

Myers PC. 2005. *Ap. J.* 623:280

Myers PC, Benson PJ. 1983. *Ap. J.* 266:309

Myers PC, Evans NJ II, Ohashi N. 2000. See Mannings et al. 2000, p. 217

Myers PC, Fuller GA, Goodman AA, Benson PJ. 1991. *Ap. J.* 376:561

Myers PC, Fuller GA, Mathieu RD, Beichman CA, Benson PJ, et al. 1987. *Ap. J.* 319:340

Myers PC, Goodman AA. 1991. *Ap. J.* 373:509

Myers PC, Mardones D, Tafalla M, Williams JP, Wilner DJ. 1996. *Ap. J. Lett.* 465:L133

Nagaoka A, Watanabe N, Kouchi A. 2005. *Ap. J. Lett.* 624:L29

Nakano T. 1998. *Ap. J.* 494:587

Nakano T, Nakamura T. 1978. *Publ. Astron. Soc. Jpn.* 30:671

Neufeld DA, Melnick GJ, Sonnentrucker P, Bergin EA, Green JD, et al. 2006. *Ap. J.* 649:816

Öberg KI, van Broekhuizen F, Fraser HJ, Bisschop SE, van Dishoeck EF, Schlemmer S. 2005. *Ap. J. Lett.* 621:L33

Ossenkopf V, Henning T. 1994. *Astron. Astrophys.* 291:943

Ossenkopf V, Mac Low MM. 2002. *Astron. Astrophys.* 390:307

Osterbrock DE. 1961. *Ap. J.* 134:270

Ostriker EC, Stone JM, Gammie CF. 2001. *Ap. J.* 546:980

Padoan P, Juvela M, Goodman AA, Nordlund Å. 2001. *Ap. J.* 553:227

Padoan P, Nordlund Å. 1999. *Ap. J.* 526:279

Pagani L, Lagache G, Bacmann A, Motte F, Cambrésy L, et al. 2003. *Astron. Astrophys.* 406:L59

Pagani L, Pardo JR, Apponi AJ, Bacmann A, Cabrit S, et al. 2005. *Astron. Astrophys.* 429:181

Palla F, Stahler SW. 2002. *Ap. J.* 581:1194

Penston MV. 1969. *MNRAS* 144:425

Perault M, Omont A, Simon G, Seguin P, Ojha D, et al. 1996. *Astron. Astrophys.* 315:L165

Pereyra A, Magalhães AM. 2004. *Ap. J.* 603:584

Pety J, Falgarone E. 2003. *Astron. Astrophys.* 412:417

Phillips TG, Vastel C. 2003. See Curry & Fich 2003, p. 3

Pillai T, Wyrowski F, Carey SJ, Menten KM. 2006. *Astron. Astrophys.* 450:569

Pineau des Forêts G, Flower DR, McCarroll R. 1991. *MNRAS* 248:173

Pontoppidan KM. 2006. *Astron. Astrophys.* 453:L47

Pontoppidan KM, van Dishoeck EF, Dartois E, Fraser HJ, Banhidi Z, Jørgensen JK, and the C2d team. 2005. See Lis et al. 2005, p. 114

Prantzos N, Aubert O. 1995. *Astron. Astrophys.* 302:69

Pratap P, Dickens JE, Snell RL, Miralles MP, Bergin EA, et al. 1997. *Ap. J.* 486:862

Rachford BL, Snow TP, Tumlinson J, Shull MJ, Blair WP, et al. 2002. *Ap. J.* 577:221

Ragan SE, Bergin EA, Plume R, Gibson DL, Wilner DJ, et al. 2006. *Ap. J. Suppl.* 166:567

Rathborne JM, Jackson JM, Simon R. 2006. *Ap. J.* 641:389

Rawlings JMC, Hartquist TW, Menten KM, Williams DA. 1992. *MNRAS* 255:471

Reipurth B. 1983. *Astron. Astrophys.* 117:183

Reipurth B, Jewitt D, Keil K, eds. 2007. *Protostars and Planets V*. Tucson, AZ: Univ. Ariz. Press

Ridge NA, Di Francesco J, Kirk H, Li D, Goodman AA, et al. 2006. *Astron. J.* 131:2921

Rieke GH, Lebofsky MJ. 1985. *Ap. J.* 288:618

Roberts H, Herbst E, Millar TJ. 2003. *Ap. J. Lett.* 591:L41

Rodríguez LF. 2005. In *The Cool Universe: Observing Cosmic Dawn*, ed. C Lidman, D Alloin, pp. 146. San Francisco: ASP

Rosolowsky EW, Goodman AA, Wilner DJ, Williams JP. 1999. *Ap. J.* 524:887

Roueff E, Tiné S, Coudert LH, Pineau des Forêts G, Falgarone E, Gerin M. 2000. *Astron. Astrophys.* 354:L63

Rybicki GB, Hummer DG. 1991. *Astron. Astrophys.* 245:171

Ryden BS. 1996. *Ap. J.* 471:822

Salpeter EE. 1955. *Ap. J.* 121:161

Sánchez N, Alfaro EJ, Pérez E. 2005. *Ap. J.* 625:849

Scalo J. 1990. In *Physical Processes in Fragmentation and Star Formation*, ed. R Capuzzo-Dolcetta, C Chiosi, A DiFazio, p. 151. Dordrecht: Kluwer

Schnee S, Goodman A. 2005. *Ap. J.* 624:254

Schneider S, Elmegreen BG. 1979. *Ap. J. Suppl.* 41:87

Shen CJ, Greenberg JM, Schutte WA, van Dishoeck EF. 2004. *Astron. Astrophys.* 415:203

Shinnaga H, Tsuboi M, Kasuga T. 1999. In *Proceedings of Star Formation 1999*, ed. T Nakamoto, p. 175. Nobeyama: Nobeyama Radio Obs.

Shu FH. 1977. *Ap. J.* 214:488

Shu FH, Adams FC, Lizano S. 1987. *Annu. Rev. Astron. Astrophys.* 25:23

Simon M. 1997. *Ap. J. Lett.* 482:L81

Simon R, Jackson JM, Rathborne JM, Chambers ET. 2006. *Ap. J.* 639:227

Skrutskie MF, Cutri RM, Stiening R, Weinberg MD, Schneider S, et al. 2006. *Astron. J.* 131:1163

Snell RL. 1981. *Ap. J. Suppl.* 45:121

Snell RL, Howe JE, Ashby MLN, Bergin EA, Chin G, et al. 2000. *Ap. J. Lett.* 539:L101

Spitzer LJ. 1978. *Physical Processes in the Interstellar Medium.* New York: Wiley

Sridharan TK, Beuther H, Saito M, Wyrowski F, Schilke P. 2005. *Ap. J. Lett.* 634:L57

Stamatellos D, Whitworth AP. 2003. *Astron. Astrophys.* 407:941

Stamatellos D, Whitworth AP, André P, Ward-Thompson D. 2004. *Astron. Astrophys.* 420:1009

Stantcheva T, Herbst E. 2003. *MNRAS* 340:983

Stark R, van der Tak FFS, van Dishoeck EF. 1999. *Ap. J. Lett.* 521:L67

Stepnik B, Abergel A, Bernard JP, Boulanger F, Cambrésy L, et al. 2003. *Astron. Astrophys.* 398:551

Stone JM, Ostriker EC, Gammie CF. 1998. *Ap. J. Lett.* 508:L99

Stutzki J, Bensch F, Heithausen A, Ossenkopf V, Zielinsky M. 1998. *Astron. Astrophys.* 336:697

Stutzki J, Güsten R. 1990. *Ap. J.* 356:513

Sun K, Kramer C, Ossenkopf V, Bensch F, Stutzki J, Miller M. 2006. *Astron. Astrophys.* 451:539

Suzuki H, Yamamoto S, Ohishi M, Kaifu N, Ishikawa SI, et al. 1992. *Ap. J.* 392:551

Swade DA. 1989. *Ap. J.* 345:828

Tachihara K, Onishi T, Mizuno A, Fukui Y. 2002. *Astron. Astrophys.* 385:909

Tafalla M, Mardones D, Myers PC, Caselli P, Bachiller R, Benson PJ. 1998. *Ap. J.* 504:900

Tafalla M, Myers PC, Caselli P, Walmsley CM. 2004. *Astron. Astrophys.* 416:191

Tafalla M, Myers PC, Caselli P, Walmsley CM, Comito C. 2002. *Ap. J.* 569:815

Tafalla M, Santiago J. 2004. *Astron. Astrophys.* 414:L53

Tafalla M, Santiago J, Myers PC, Caselli P, Walmsley CM, Crapsi A. 2006. *Astron. Astrophys.* 455:577

Testi L, Sargent AI. 1998. *Ap. J. Lett.* 508:L91

Teyssier D, Hennebelle P, Pérault M. 2002. *Astron. Astrophys.* 382:624

Tielens AGGM. 1983. *Astron. Astrophys.* 119:177

Tielens AGGM. 2005. *The Physics and Chemistry of the Interstellar Medium.* Cambridge, UK: Cambridge Univ. Press

Tielens AGGM, Hagen W. 1982. *Astron. Astrophys.* 114:245

Tomisaka K, Ikeuchi S, Nakamura T. 1988. *Ap. J.* 335:239

Tóth LV, Haas M, Lemke D, Mattila K, Onishi T. 2004. *Astron. Astrophys.* 420:533

Troland TH, Crutcher RM, Goodman AA, Heiles C, Kazes I, Myers PC. 1996. *Ap. J.* 471:302

Turner BE, Heiles C. 2006. *Ap. J. Suppl.* 162:388

van der Tak FFS, Caselli P, Ceccarelli C. 2005. *Astron. Astrophys.* 439:195

van Dishoeck EF. 2004. *Annu. Rev. Astron. Astrophys.* 42:119

van Dishoeck EF, Blake GA. 1998. *Annu. Rev. Astron. Astrophys.* 36:317

Vastel C, Phillips TG, Yoshida H. 2004. *Ap. J. Lett.* 606:L127

Vázquez-Semadeni E. 1994. *Ap. J.* 423:681

Vázquez-Semadeni E, Ballesteros-Paredes J, Klessen RS. 2003. *Ap. J. Lett.* 585:L131

Walmsley CM, Flower DR, Pineau des Forêts G. 2004. *Astron. Astrophys.* 418:1035

Walmsley CM, Ungerechts H. 1983. *Astron. Astrophys.* 122:164

Walsh AJ, Myers PC, Burton MG. 2004. *Ap. J.* 614:194

Ward-Thompson D, André P, Crutcher R, Johnstone D, Onishi T, Wilson C. 2007. See Reipurth et al. 2007, p. 33

Ward-Thompson D, André P, Kirk JM. 2002. *MNRAS* 329:257

Ward-Thompson D, Kirk JM, Crutcher RM, Greaves JS, Holland WS, André P. 2000. *Ap. J. Lett.* 537:L135

Ward-Thompson D, Motte F, André P. 1999. *MNRAS* 305:143

Ward-Thompson D, Scott PF, Hills RE, André P. 1994. *MNRAS* 268:276

Weingartner JC, Draine BT. 2001. *Ap. J. Suppl.* 134:263

Weinreb S, Barrett AH, Meeks ML, Henry JC. 1963. *Nature* 200:829

Werner M, Fazio G, Rieke G, Roellig TL, Watson DM. 2006. *Annu. Rev. Astron. Astrophys.* 44:269

Whittet DCB, Bode MF, Longmore AJ, Adamson AJ, McFadzean AD, et al. 1988. *MNRAS* 233:321

Whittet DCB, Gerakines PA, Hough JH, Shenoy SS. 2001. *Ap. J.* 547:872

Whittet DCB, Shenoy SS, Bergin EA, Chiar JE, Gerakines PA, et al. 2007. *Ap. J.* 655:332

Whitworth AP, Ward-Thompson D. 2001. *Ap. J.* 547:317

Willacy K, Langer WD, Velusamy T. 1998. *Ap. J. Lett.* 507:L171

Williams JP, Bergin EA, Caselli P, Myers PC, Plume R. 1998. *Ap. J.* 503:689

Williams JP, Blitz L, McKee CF. 2000. See Mannings et al. 2000, p. 97

Williams JP, de Geus EJ, Blitz L. 1994. *Ap. J.* 428:693

Williams JP, Myers PC, Wilner DJ, di Francesco J. 1999. *Ap. J. Lett.* 513:L61

Wilson RW, Jefferts KB, Penzias AA. 1970. *Ap. J. Lett.* 161:L43

Wolf S, Launhardt R, Henning T. 2003. *Ap. J.* 592:233

Young CH, Jørgensen JK, Shirley YL, Kauffmann J, Huard T, et al. 2004. *Ap. J. Suppl.* 154:396

Young KE, Enoch ML, Evans NJ II, Glenn J, Sargent A, et al. 2006. *Ap. J.* 644:326

Yun JL, Clemens DP. 1990. *Ap. J. Lett.* 365:L73

Zhou S, Wu Y, Evans NJ II, Fuller GA, Myers PC. 1989. *Ap. J.* 346:168

Zucconi A, Walmsley CM, Galli D. 2001. *Astron. Astrophys.* 376:650

Zuckerman B, Evans NJ II. 1974. *Ap. J. Lett.* 192:L149